



Published in final edited form as:

*Q J Nucl Med Mol Imaging*. 2015 September ; 59(3): 241–268.

## Prostate-specific membrane antigen as a target for cancer imaging and therapy

A. P. KIESS<sup>1,\*</sup>, S. R. BANERJEE<sup>2,\*</sup>, R. C. MEASE<sup>2</sup>, S. P. ROWE<sup>2</sup>, A. RAO<sup>1</sup>, C. A. FOSS<sup>2</sup>, Y. CHEN<sup>2</sup>, X. YANG<sup>2</sup>, S. Y. CHO<sup>3</sup>, S. NIMMAGADDA<sup>2</sup>, and M. G. POMPER<sup>1,2</sup>

<sup>1</sup>Department of Radiation Oncology, Johns Hopkins Medical Institutions, Baltimore, MD, USA

<sup>2</sup>The Russell H. Morgan Department of Radiology and Radiological Science, Johns Hopkins Medical Institutions, Baltimore, MD, USA

<sup>3</sup>Department of Radiology, University of Wisconsin School of Medicine and Public Health, Madison, WI, USA

### Abstract

The prostate-specific membrane antigen (PSMA) is a molecular target whose use has resulted in some of the most productive work toward imaging and treating prostate cancer over the past two decades. A wide variety of imaging agents extending from intact antibodies to low-molecular-weight compounds permeate the literature. In parallel there is a rapidly expanding pool of antibody-drug conjugates, radiopharmaceutical therapeutics, small-molecule drug conjugates, theranostics and nanomedicines targeting PSMA. Such productivity is motivated by the abundant expression of PSMA on the surface of prostate cancer cells and within the neovasculature of other solid tumors, with limited expression in most normal tissues. Animating the field is a variety of small-molecule scaffolds upon which the radionuclides, drugs, MR-detectable species and nanoparticles can be placed with relative ease. Among those, the urea-based agents have been most extensively leveraged, with expanding clinical use for detection and more recently for radiopharmaceutical therapy of prostate cancer, with surprisingly little toxicity. PSMA imaging of other cancers is also appearing in the clinical literature, and may overtake FDG for certain indications. Targeting PSMA may provide a viable alternative or first-line approach to managing prostate and other cancers.

### Keywords

Positron-emission tomography; Diagnosis; Molecular imaging; Prostate cancer; Theranostic

---

Accurate diagnosis, staging, and therapeutic monitoring in patients with cancer are the most important goals of oncologic imaging. Those goals are often well served with functional/metabolic imaging, particularly within the realm of nuclear medicine with positron-emission

---

Corresponding author: M. G. Pomper, Johns Hopkins Medical School, 1550 Orleans St., CRB II 492, Baltimore, MD 21287, USA. mpomper@jhmi.edu.

\*Equal contribution

*Conflicts of interest.* The authors certify that there is no conflict of interest with any financial organization regarding the material discussed in the manuscript.

tomography (PET) and single-photon emission computed tomography (SPECT), leveraging a variety of radiolabeled compounds. PET imaging with 2-deoxy-2-[<sup>18</sup>F]fluoroglucose (FDG) has proven to be transformative in oncologic imaging in recent decades.<sup>1-4</sup> However, FDG PET has profound limitations in imaging certain malignancies including prostate cancer,<sup>5-7</sup> spurring the need for development of new radiotracers able to address these limitations. That is illustrated, in part, by the emergence of numerous PET and SPECT radiotracers targeting the prostate-specific membrane antigen (PSMA).

Conventional imaging of primary prostate cancer is generally performed with magnetic resonance (MR) imaging, with conventional imaging of metastatic or recurrent prostate cancer centered around contrast-enhanced computed tomography (CT) and bone scan with <sup>99m</sup>Tc-methylene diphosphonate (MDP). MR imaging can be non-specific in the context of primary prostate cancer, with benign prostatic hyperplasia at times having similar imaging characteristics to malignant tissue.<sup>8</sup> Both CT and bone scan have limitations in sensitivity and specificity for the detection of early/subtle recurrence or metastasis, *e.g.*, sub-centimeter, disease-involved lymph nodes and sclerotic bone metastases. High-affinity radiotracers targeting PSMA could potentially address those limitations.

PSMA represents an excellent target for molecular imaging of prostate cancer. PSMA is a type II membrane metalloenzyme that exhibits developmentally controlled and tissue-specific expression patterns (Figure 1).<sup>9</sup> Expression on the plasma membrane is restricted to a few healthy tissues such as lacrimal and salivary glands, proximal renal tubules, epididymis, ovary, the luminal side of the ileum-jejunum and astrocytes within the central nervous system (CNS); healthy prostate gland expresses comparatively little PSMA, which is confined within the apical epithelium of secretory ducts.<sup>10-12</sup> In these non-malignant tissues, uptake of PSMA-targeted probes may be limited by an intact blood-brain barrier, a healthy proximal small bowel lumen, and truncated cytoplasmic expression of PSMA within normal prostate. PSMA within prostate cancer cells begins to up-regulate and migrate to the plasma membrane during the transition to androgen independence, and is most associated with high grade, metastatic disease.<sup>13-16</sup> Nevertheless, PSMA is expressed in most primary prostate tumors as well, regardless of androgen status.<sup>17,18</sup>

Because the active site of PSMA is highly conserved,<sup>19</sup> the development of molecular probes binding with high affinity and specificity to the active site is an efficient strategy that avoids dependence on glycosylation patterns<sup>20-22</sup> and other post-translational, cell-specific processing, which may be subject to the tumor microenvironment. The caveolin-dependent, rapid internalization of PSMA while bound as a dimer to its ligand<sup>23</sup> is also a desirable feature of this target, as well as its final peri-nuclear localization.<sup>24,25</sup> Endogenous substrates include dietary poly- $\gamma$ -glutamyl folates<sup>26,27</sup> and *N*-acetylaspartyl glutamate (NAAG, within CNS),<sup>28,29</sup> but the function and identity of other ligands is a topic of speculation. PSMA is also expressed within the neovascular endothelium of most solid tumors,<sup>30-34</sup> enabling imaging of a variety of malignancies with probes targeted toward PSMA.

This review will provide a detailed account of the structure-based design of small-molecule PSMA inhibitors, including radiohalogenated agents and radiometals for radionuclide imaging, as well as other PSMA-targeted agents for optical and MR imaging. It will then

describe the clinical experience to date with PSMA-targeted radionuclide imaging and the emergence of potential PSMA-targeted therapies and theranostic agents.

## Structure-based design of small-molecule PSMA inhibitors

The high expression of PSMA (EC 3.4.17.21), *a.k.a.*, glutamate carboxypeptidase II (GCPII), *N*-acetyl-L-aspartyl-L-glutamate peptidase I or NAAG peptidase, on the surface of prostate cancer cells and on most tumor neovasculature has rendered it a useful and popular target for molecular imaging. Small-molecule PSMA inhibitors are zinc binding compounds attached to a glutamate or glutamate isostere and fall into three families: 1) phosphonate-, phosphate-, and phosphoramidate compounds; 2) thiols; and 3) ureas.<sup>35,36</sup> Initial phosphonate and phosphate inhibitors were prepared at ZENECA and later at Guilford Pharmaceuticals,<sup>37,38</sup> and phosphoramidate compounds were reported by Berkman *et al.*<sup>39–41</sup> Urea-based compounds designed to inhibit GCPII in the brain were first reported by Kozikowski *et al.*<sup>42,43</sup> Low-molecular-weight agents for imaging and therapy of PSMA prepared to date have been either ureas or phosphoramidates, with the majority having been based on the urea scaffold. Those agents possess a terminal glutamate or glutamate isostere at the P1' position, which enables productive binding to PSMA, and are amenable to modification with bulky substituents that interact with the arginine patch or tunnel region of PSMA.

Recent crystallographic studies of complexes between PSMA and low-molecular-weight ligands elucidated their binding modes within the active site of PSMA, revealing that the S1 pocket of PSMA is more tolerant toward structural modification than the glutamate-binding S1' (pharmacophore) pocket.<sup>44</sup> There is also a deep, funnel-shaped accessory tunnel that contains several more exosites that could be exploited in design of more potent inhibitors. Barinka *et al.* reported the first detailed structures of complexes between human PSMA and urea-based inhibitors and identified a hydrophobic accessory pocket near the S1 site.<sup>45</sup> That pocket produced an unusually high binding interaction with 2-[3-[1-carboxy-5-(4-iodo-benzoylamino)-pentyl]-ureido]-pentanedioic acid (DCIBzL) (Table I, Entry 5), one of the most potent urea-based inhibitors of PSMA synthesized to date ( $K_i=0.01$  nM).<sup>46</sup> The crystal structure of PSMA complexed with DCIBzL (PDB ID: 3D7H) revealed that the iodophenyl group of DCIBzL projects into the arginine patch region and resides in the accessory pocket created by side chains of arginines 463, 534 and 536 (Figure 2).<sup>45</sup> The hydrophobic pocket accessory to the S1 site has recently been exploited for structure-based design of new PSMA inhibitors to improve binding affinity and pharmacokinetic properties.<sup>47–49</sup>

In another approach, Zhang *et al.* identified and structurally characterized another exosite of PSMA that binds aromatic moieties.<sup>50</sup> That exosite, termed the arene-binding site, is formed by the indole group of Trp541 and the guanidinium group of Arg511. Attaching a dinitrophenyl moiety with a length-optimized linker to a PSMA inhibitor significantly enhanced affinity toward PSMA through the avidity effect of the arene-binding site, namely, by allowing it to bind to PSMA in a bi-dentate mode by interacting with both S1' and S1 pockets.

## Radiolabeled small-molecule PSMA inhibitors for radionuclide imaging

We have divided this topic into two sections, one focusing on radiohalogenated agents and the other on those employing radiometals, rather than by modality. That reflects the possibility of a particular scaffold being used for more than one modality.

### Radiohalogenated agents

A list of radiohalogenated and  $^{11}\text{C}$ -labeled small-molecule PSMA inhibitors is presented in Table I. The first reported radiolabeled small-molecule PSMA inhibitor for PET imaging was the methyl cysteine-glutamate urea,  $^{11}\text{C}$ MCG, a.k.a., *N*-[*N*-[(*S*)-1,3-dicarboxypropyl]carbamoyl]-*S*- $^{11}\text{C}$ methyl-L-cysteine, or  $^{11}\text{C}$ DCMC, (Table I, Entry 1), which demonstrated PSMA-specific uptake in mouse and non-human primate kidney<sup>51</sup> and in PSMA+ LNCaP tumor xenografts.<sup>52</sup> Foss and coworkers demonstrated that a radiohalogenated small-molecule PSMA inhibitor, the iodotyrosine-glutamate urea *N*-[*N*-[(*S*)-1,3-dicarboxypropyl]carbamoyl]-*S*-3- $^{125}\text{I}$ iodo-L-tyrosine,  $^{125}\text{I}$ DCIT (Table I, Entry 2), also showed PSMA-specific uptake in PSMA+ LNCaP tumor xenografts.<sup>52</sup> Expanding to  $^{18}\text{F}$ , that same group synthesized *N*-[*N*-[(*S*)-1,3-dicarboxypropyl]carbamoyl]-4- $^{18}\text{F}$ fluorobenzyl-L-cysteine ( $^{18}\text{F}$ DCFBC) (Table I, Entry 3) to leverage the salutary characteristics of this isotope for PET and clinical translation.<sup>53</sup>  $^{18}\text{F}$  DCFBC enabled visualization of PSMA+ PC3 PIP tumor xenografts with low normal organ uptake except for kidney and accumulation within bladder. A second generation agent, 2-(3-(1-carboxy-5-[(6- $^{18}\text{F}$ ) fluoro-pyridine-3-carbonyl)-amino]-pentyl)-ureido)-pentanedioic acid [ $^{18}\text{F}$ ]DCFpyL (Table I, Entry 11), which contains a 6- $^{18}\text{F}$ fluoronicotinamido group on a lysine-glutamate urea, gave higher tumor to normal tissue ratios compared to [ $^{18}\text{F}$ ]DCFBC in PSMA+ PC3 PIP tumor xenografts (Figure 3).<sup>54</sup> Other  $^{18}\text{F}$ -labeled, aryl substituted lysine glutamate ureas have been prepared (Table I, Entries 4, 12, 13, 14, 25, 26).<sup>46,55,56</sup> Substituted Glu-Glu ureas have also been radiolabeled with  $^{18}\text{F}$ . Those include a 6- $^{18}\text{F}$  fluoronicotinamido substituted linker-Glu-Glu urea (Table I, Entry 15),<sup>57</sup> Al $^{18}\text{F}$ -2,2',2''-(1,4,7-triazonane-1,4,7-triyl) triacetic acid (NOTA) linker-Glu-Glu ureas (Table I, Entries 17 and 23),<sup>58,59</sup> and Al $^{18}\text{F}$ -2-[2-[carboxymethyl-[(2-hydroxyphenyl)methyl] amino]ethyl-[(2-hydroxyphenyl)methyl]amino]acetic acid (HBED)-linker-Glu-Glu urea (Table I, Entry 24).<sup>60</sup>  $^{18}\text{F}$ -Labeled Phe-Glu ureas (Table I, Entries 19 and 20) have also been prepared.<sup>61,62</sup> Compound P238 (Table I, Entry 20) is dimeric with a high affinity for PSMA ( $K_i=0.1-0.4$  nM), and demonstrated high specific uptake in PSMA+ LNCaP tumor xenografts with fast clearance from normal tissues through the kidneys.<sup>63</sup> Two  $^{18}\text{F}$ -labeled phosphoramidates (Table I, Entries 10 and 27) have been reported.<sup>64,65</sup> Both agents demonstrated specific uptake in PSMA expressing tumor xenografts with fast clearance from normal tissues. An  $^{18}\text{F}$ -labeled derivative (Table I, Entry 18) of the potent PSMA inhibitor 2-(phosphonomethyl)pentandioic acid (2-PMPA) has also been reported.<sup>66</sup> Although that agent clearly visualized PSMA+ LNCaP tumor xenografts, the images also showed significant bone uptake likely due its phosphonate structure.<sup>67</sup> Several radioiodinated Lys-Glu urea derivatives have been reported that utilized different radioiodinated prosthetic groups. Those include the 4-iodo-benzoyl group (Table I, Entry 5),<sup>46</sup> the 5-iodo-3-carbonyl-pyridine group (Table I, Entry 6),<sup>46</sup> the 4-iodo-benzyl group (Table I, Entry 7),<sup>68, 69</sup> the 4-iodo-phenyl-ureido group (Table I, Entry 8)<sup>68, 69</sup> and an iodotriazole (Table I, Entry 16).<sup>70</sup> All of those

radioiodinated agents demonstrated specific uptake in PSMA expressing tumor xenografts and roughly similar normal organ biodistribution with the exception of the iodotriazole compound (Table I, Entry 16), which had significant uptake in the thyroid (10% of the injected dose per gram of tissue [% ID/g] at 23 hours postinjection). Compounds MIP-1072 (Table I, Entry 7) and MIP-1095 (Table I, Entry 8) have also been radiolabeled with  $^{123}\text{I}$  and translated to clinical imaging where they enabled detection of metastatic prostate cancer with high sensitivity.<sup>71</sup> MIP-1095 has also been prepared with  $^{124}\text{I}$  for PET imaging and with  $^{131}\text{I}$  for radiopharmaceutical therapy, with clinical trials ongoing, as discussed below.<sup>72</sup>

## Radiometals

Several classes of PSMA-based, radiometal-labeled imaging agents using Lys-Glu-urea as the targeting scaffold have been reported. To provide high-affinity agents, Banerjee *et al.*, envisioned the need to attach a linker between a bulky metal chelator and the PSMA-targeting urea moiety, allowing the urea to reach the binding site while keeping the bulky metal chelated part on the exterior of the enzyme active site (Figure 4). By employing that targeting strategy they have synthesized a series of SPECT imaging agents using both  $^{99\text{m}}\text{Tc}^{\text{I}}(\text{CO})_3$  and  $^{99\text{m}}\text{Tc}^{\text{VO}^{+3}}$  labeling techniques and several well-studied chelating agents related to the individual coordination chemistry required for these two species (Table II, Entries 2–4, 11–12).<sup>73, 74</sup> Although most of those agents demonstrated high uptake and retention in PSMA expressing xenografts, the choice of chelating agent was found to have a moderate to significant effect on the overall pharmacokinetics. Low *et al.* reported a series of  $^{99\text{m}}\text{Tc}$ -Oxo-labeled agents, the lead agent (Table II, Entry 5) having been prepared using bis-Glu urea as the targeting moiety.<sup>75</sup> Those compounds showed specific uptake in PSMA expressing xenografts. Babich *et al.* investigated a series of  $^{99\text{m}}\text{Tc}$  and Re-tricarbonyl-based agents using both Lys-Glu as well as Glu-Glu ureas as targeting scaffolds with different chelating agents having different degrees of hydrophilicity (Table II, Entries 7, 9–10).<sup>76–78</sup> Agent  $^{99\text{m}}\text{Tc}$ MIP-1404 exhibited the best combination of high tumor uptake and rapid clearance from kidney and non-target tissues by four hours post-injection.<sup>77, 78</sup> Phosphoramidate-based inhibitors were also investigated using the  $^{99\text{m}}\text{Tc}$ -tricarbonyl-core and 2-[bis[2-[bis(carboxymethyl)amino]ethyl]amino]acetic acid (DTPA) and bis(pyridin-2-ylmethyl)amine (DPA) as chelating agents (Table II, Entries 6 and 8).<sup>79, 80</sup> Misra and coworkers reported a simple solid phase, cartridge-based method to prepare  $^{99\text{m}}\text{Tc}$ - S-acetylmercaptoacetyltriserine-NHS from  $^{99\text{m}}\text{TcO}_4^-$  to ~99% radiochemical purity.<sup>81</sup> The radiolabeled intermediate was then conjugated to negatively charged adamantane-trimerized 2[(3-ami-no-3-carboxypropyl)(hydroxy)(phosphinyl)-methyl] pentane-1,5-dioic acid (GPI) in one step without the need for purification by high performance liquid chromatography to produce  $^{99\text{m}}\text{Tc}$ -labeled agents (Table II, Entry 1). PSMA-specific cell binding was verified but no *in vivo* data are available.

Using the linker-urea PSMA-targeting construct, Banerjee *et al.*, have extended their work to explore generator-produced  $^{68}\text{Ga}$  for PET imaging and reported the synthesis and testing of the  $^{68}\text{Ga}$ -labeled PSMA-targeted imaging agents depicted in Table III, Entries 1–2.<sup>82</sup> They chose the commercially available macrocyclic chelating agent DOTA-monoamide so that the agents could be used for both imaging and therapeutic applications. The lead agent from that initial study, [ $^{68}\text{Ga}$ ]6 (Entry 2), demonstrated uptake in PSMA+ PC3 PIP tumors at 45

minutes post-injection with little visible uptake in PSMA-PC3 flu xenografts.<sup>82</sup> That agent also showed fast renal clearance while maintaining high PSMA+ tumor retention with tumor to muscle and tumor to blood ratios of 110 and 22, respectively. Eder *et al.* reported [<sup>68</sup>Ga]DKFZ-PSMA-11, *i.e.* <sup>68</sup>Ga-PSMA, Table III, Entry 9),<sup>83</sup> using the chelator *N,N*-bis[2-hydroxy-5-(carboxyethyl)-benzyl]ethylenediamine-*N,N*-diacetic acid (HBED-CC), an analog of HBED.<sup>84–87</sup> HBED is a potentially more attractive chelator for <sup>68</sup>Ga because it forms a more thermodynamically stable complex than does DOTA (logK<sub>ML</sub> of 35.6 vs. 21.3 for DOTA)<sup>87</sup>. Furthermore, DKFZ-PSMA-11 can be radiolabeled with <sup>68</sup>Ga(III) at room temperature in less than five minutes in high yield and purity. When similar post-radiolabeling purification schemes for [<sup>68</sup>Ga]6 (Table III, Entry 2)<sup>82</sup> and [<sup>68</sup>Ga]DKFZ-PSMA-11 were employed, the two compounds displayed similar uptake and retention in PSMA+ PC3 PIP tumors, although significantly higher tumor to kidney, tumor to spleen, and tumor to salivary gland ratios were observed for [<sup>68</sup>Ga]6.<sup>89</sup> A recent report by Eder and coworkers (Table III, Entry 15) also showed rapid renal clearance and normal tissue uptake of the <sup>68</sup>Ga-DOTA-mono amide analog [<sup>68</sup>Ga]PSMA-617 compared to [<sup>68</sup>Ga]DKFZ-PSMA-11, which bears the HBED-CC chelator.<sup>90</sup> That group has also used the HBED-CC chelator in a <sup>68</sup>Ga-labeled hetero-bivalent compound designed to target both PSMA and gastrin-releasing peptide, and have demonstrated dual-targeted PET imaging in pre-clinical models.<sup>91</sup>

Banerjee *et al.* have also investigated the cyclotron-produced, long-lived (T<sub>1/2</sub>=12.7 hours) radionuclide <sup>64</sup>Cu for PET imaging of PSMA<sup>92</sup> by utilizing different macrocyclic chelating agents as shown in Table II, Entries 13 and 14. The agent conjugated with the 4,8,11-tetraazabicyclo[6.6.2]hexadecane-4,11-diacetic acid (CB-TE2A) chelator (Table II, Entry 14), demonstrated improved biodistribution with rapid clearance from normal tissues, including kidney, within two hours post-injection, resulting in high image contrast. Such an agent may be useful to detect minute metastatic lesions. A <sup>64</sup>Cu-labeled dual-targeting agent that binds to PSMA and gastrin-releasing peptide receptors (GRPr) was recently reported using Glu-Glu urea as the targeting moiety for PSMA and BBN(7–14)NH<sub>2</sub> for GRPr with NODAGA as a chelating agents<sup>93</sup> <sup>64</sup>Cu-Labeled PSMA-targeted agents using GPI as the targeting moiety and (CB-TE2A) as the chelator are also known.<sup>94</sup> Moreover, 1,4,7-triazacyclononane-1,4,7-tris(2-carboxyethyl-methylenephosphinic acid (TRAP) has been used as a chelating agent/scaffold for <sup>64</sup>Cu and <sup>68</sup>Ga-labeled PSMA-targeted PET agents. A trimeric PSMA-targeted TRAP(DUPA-Pep)<sub>3</sub> was shown to provide higher image contrast than a monomeric analog, although renal uptake of the former was higher.<sup>95</sup>

## PSMA-targeted optical and MR imaging agents

### Optical agents

*In vivo* optical imaging with; probes that emit in the near-infrared (NIR) region of the electromagnetic spectrum is a rapidly emerging technology. Near-infrared fluorescence imaging is highly sensitive, non-invasive, inexpensive, and has significant potential to enhance real-time, image-guided surgery, specifically for assuring negative surgical margins.<sup>96, 97</sup> A wide variety of low-molecular-weight, PSMA-targeted optical imaging agents have been reported and are summarized in Table IV. Humblet *et al.* reported the first



PSMA-targeted mono- and multivalent NIR GPI derivatives.<sup>98, 99</sup> Rapid clearance of the monomeric compound from the blood limited the time required for productive engagement of PSMA-expressing tumor,<sup>98</sup> and *in vivo* results were not reported for the corresponding multivalent compounds.<sup>99</sup> Liu *et al.* have labeled PSMA inhibitors that employed the phosphoramidate and phosphate scaffold and demonstrated their PSMA-binding specificity and intracellular localization *in vitro*, but *in vivo* imaging results have not been reported.<sup>40, 100, 101</sup> Banerjee and coworkers synthesized an early urea-based fluorescent compound, ReL2 (Table IV, Entry 11), but *in vivo* images were not obtained as the fluorophore would have an insufficient depth of penetration to be detected.<sup>73</sup> Utilizing the same Glu-Lys-urea scaffold, Chen and coworkers reported YC-27 (Table IV, Entry 12), which enabled visualization of PSMA-expressing xenografts in mice.<sup>102</sup> They extended that work by synthesizing and testing a series of compounds using different fluorophores and linkers (Table IV, Entries 12–26). The imaging results further confirmed that a linker of appropriate length between the PSMA-binding urea and the bulky fluorophore was critical for productive PSMA targeting *in vivo* for this class of agents.<sup>103</sup> Neuman *et al.* have recently used YC-27 to demonstrate the utility of NIRF for assurance of negative margins in pre-clinical models of PC<sup>104</sup> (Figure 5). Kularatne,<sup>75</sup> Kelderhouse<sup>105</sup> and Wang<sup>106</sup> have synthesized a series of optical agents utilizing the Glu-Glu-urea scaffold with different linkers and demonstrated that these compounds also bind selectively to PSMA. Other preclinical agents with an optical component including hetero-bivalent compounds targeting both PSMA and integrin  $\alpha_v\beta_3$  (Table IV, Entry 27),<sup>107</sup> as well as dual modality agents which enable sequential SPECT and optical<sup>108</sup> and bionized nanoferrite (BNF) nanoparticles for optical and SPECT imaging.<sup>109</sup>

## MR agents

MR molecular imaging can combine the ubiquity of this established clinical modality and its high spatial resolution with molecular profiling *in vivo*. However, due to the intrinsically low sensitivity of MR, nanoparticles are often employed as a platform to improve sensitivity, specifically for imaging receptors. The use of PSMA-targeted iron oxide nanoparticles as T<sub>2</sub>-contrast agents has been investigated by several groups recently by employing either aptamer or antibody targeting.<sup>110–115</sup> Abdolahi and coworkers evaluated J591-conjugated superparamagnetic iron-oxide magnetic nanoparticles (SPIONs) that displayed specific T<sub>2</sub> MR contrast enhancement of PSMA+ LNCaP cells but not of PSMA- DU145 cells.<sup>113</sup> Magnetic nanoparticles (MNPs) conjugated to the PSMA-targeted antibody J591 were shown to invoke PSMA-specific MR contrast enhancement in a preclinical model of orthotopic prostate cancer.<sup>114</sup> Administration of J591-MNP conjugates resulted in significant darkening of the T<sub>2</sub>-weighted MR images within the region of the prostate at two and 24 hours post-injection compared to mice given untargeted MNPs. Recently, a PSMA-targeted polypeptide, CQKHHNYLC C1–C9 disulfide, was conjugated to the surface of a new SPION formulation for PSMA-specific MR imaging.<sup>115</sup> In LNCaP tumor-bearing mice injected with polypeptide-SPIONs, T<sub>2</sub> signal reduction within tumors was observed from two to 12 hours post-injection. No appreciable tumor signal changes were observed in the control groups at any time point. As opposed to those nanoparticle-based T<sub>2</sub> contrast agents, Banerjee *et al.* have recently reported Gd(III)-based low-molecular-weight T<sub>1</sub>-contrast agents weighted to provide positive contrast enhancement.<sup>116</sup> Three high-affinity, low-

molecular-weight gadolinium(Gd)(III)-based PSMA-targeted contrast agents containing one to three Gd-chelates per molecule (Gd1–Gd3) were synthesized employing a PSMA-targeted Glu-Lys-urea-linker construct. They evaluated the relaxometric properties of those agents in solution, in prostate cancer cells and in an *in vivo* experimental model to demonstrate the feasibility of T<sub>1</sub>-weighted, PSMA-based MR contrast enhancement (Figure 6). *In vivo* MR imaging of Gd3 in mice bearing PSMA+ PC3 PIP and PSMA- PC3 flu tumors showed ~36% enhancement in PSMA+PC3 PIP tumor at 30 minutes post-injection and remained high with ~25% enhancement at three hours, whereas PSMA- PC3 flu tumor showed rapid decay in signal intensity after an initial ~24% enhancement at 30 minutes at 9.4 T. Other mice dosed in the same fashion using a trimeric Gd-probe without a targeting moiety,<sup>117</sup> showed no significant tumor enhancement at similar time points. They concluded that PSMA is expressed in sufficient quantities on cells to enable MR-based targeting, using only modest signal enhancement built into the imaging agent.

### PSMA-targeted detection of human prostate cancer

Diagnostic imaging of prostate cancer by targeting PSMA is not a new concept. The first radiotracer to target PSMA and find clinical applicability was <sup>111</sup>In-capromab pentetide (ProstaScint<sup>®</sup>, Cytogen Corporation, Princeton, NJ, USA), a mouse monoclonal antibody conjugate that can be imaged using SPECT, the target epitope of which is an intracellular domain of PSMA.<sup>118–120</sup> Although ProstaScint<sup>®</sup> imaging has been used extensively in the context of recurrent metastatic prostate cancer that was occult on conventional anatomic imaging, ultimately the necessity for PSMA-expressing prostate cancer cells to be lysed with exposure of the cytoplasmic target epitope,<sup>118–120</sup> as well as the limited spatial resolution of the SPECT acquisition and relatively high blood pool activity of the radiolabeled antibody, limited the utility of this agent.

New monoclonal antibodies and antibody derivatives targeted to PSMA have also been examined. The most extensively studied of those is the J591 antibody to the extracellular domain of PSMA. An analysis of a total of 53 patients imaged with either <sup>111</sup>In- or <sup>177</sup>Lu-labeled J591 found that 98% of patients with demonstrable metastatic prostate cancer had lesions that were targeted by the antibody.<sup>121</sup> A <sup>89</sup>Zr-labeled conjugate of the J591 antibody has also been synthesized for use as a PET radiotracer for imaging prostate cancer. A recent prospective study in patients awaiting prostatectomy found that this agent was able to identify tumors with a Gleason score of 7 or greater.<sup>122</sup> A phase I imaging trial with a <sup>89</sup>Zr-labeled, engineered fragment of J591 (<sup>89</sup>Zr-huJ591) in 10 patients with metastatic prostate cancer demonstrated the ability of this construct to identify metastases, including lesions that were not noted on conventional imaging.<sup>123</sup>

One of the primary shortcomings of antibody-based imaging is the long time from injection to optimal imaging time, with several days often required. That in turn limits the choice of usable radioisotopes to those with relatively long half-lives. To address that issue, multiple small-molecule ligands targeting PSMA have also been explored, as detailed in the previous sections. Among the early small-molecule PSMA ligands tested in human subjects were a pair of <sup>123</sup>I-labeled agents, <sup>123</sup>I-MIP-1072 and <sup>123</sup>I-MIP-1095, which have been found to localize to sites of metastatic prostate cancer in both bone and soft tissue.<sup>71</sup> Agents <sup>99m</sup>Tc-



MIP-1404 and  $^{99m}\text{Tc}$ -MIP-1405 (Table II, Entry 10) were investigated in six healthy men and six men with radiographic evidence of metastatic prostate cancer.<sup>124</sup> Compared to standard MDP bone scanning, both agents identified most bone metastatic lesions and rapidly detected soft-tissue lesions including sub-centimeter lymphnodes.

Cho *et al.* used [ $^{18}\text{F}$ ]DCFBC, a first-generation  $^{18}\text{F}$ -labeled urea, in a first-in-man study of PSMA-targeted PET.<sup>125</sup> [ $^{18}\text{F}$ ]DCFBC enabled detection of sites of metastatic prostate cancer in bone and lymph nodes. [ $^{18}\text{F}$ ]DCFBC has subsequently been shown to be capable of imaging primary prostate cancer with radiotracer uptake correlating to Gleason Score,<sup>126</sup> which might allow for better selection of patients who should undergo surgery or radiation *versus* those who should undergo active surveillance. That agent has been found to image metastatic prostate cancer reliably in both hormone-sensitive and castration-resistant patients. Szabo *et al.* have also recently published a first-in-man experience with a second generation, higher-affinity PSMA-targeted radiotracer, [ $^{18}\text{F}$ ]DCFpyL, which demonstrated lower blood pool activity, higher tumor uptake, and markedly improved tumor to background ratios in comparison to [ $^{18}\text{F}$ ]DCFBC<sup>127</sup> (Figure 7). [ $^{18}\text{F}$ ]DCFpyL showed maximum tumor standardized uptake values ( $\text{SUV}_{\text{max}}$ ) as high as 100 at 2 to 2.5 hours post-injection. Another radiofluorinated agent, (2*RS*,4*S*)-2- $^{18}\text{F}$ -fluoro-4-phosphonomethyl-pentanedioic acid (BAY1075553), was found by Beheshti and coworkers to be able to detect primary and metastatic sites of prostate cancer, although there were reported limitations in both sensitivity and specificity.<sup>128</sup>

Outside of those  $^{18}\text{F}$ -labeled agents, a great deal of clinical experience has been gained in Europe utilizing a  $^{68}\text{Ga}$ -labeled, urea-based compound, referred to as  $^{68}\text{Ga}$ -PSMA, *i.e.*, [ $^{68}\text{Ga}$ ]DKFZ-PSMA-11 (Table III, Entry 10).<sup>83, 129</sup>  $^{68}\text{Ga}$  has the distinct advantage of being generator-produced, allowing it to be used at sites without ready access to a medical cyclotron. However, relative to  $^{18}\text{F}$ ,  $^{68}\text{Ga}$  has a shorter physical half-life (68 minutes *versus* 110 minutes) that limits its ability to be produced at a central location and shipped to other sites and  $^{68}\text{Ga}$  also produces higher energy positrons that, in theory, degrade its spatial resolution.<sup>130</sup> Nevertheless, a number of studies and case reports have been published that demonstrate that the  $^{68}\text{Ga}$  ligands are able to detect prostate and other cancers reliably in a variety of contexts. A study of 37 patients with biochemically recurrent prostate cancer demonstrated a higher lesion detection rate with  $^{68}\text{Ga}$ -PSMA PET/CT in comparison to  $^{18}\text{F}$ -fluoromethylcholine PET/CT.<sup>131</sup> A large retrospective analysis of 319 patients with biochemical recurrence found that  $^{68}\text{Ga}$ -PSMA was able to detect sites of disease in 82.8%, with reported sensitivity, specificity, negative predictive value, and positive predictive value on a lesion-by-lesion basis of 76.6%, 100%, 91.4%, and 100%, respectively.<sup>132</sup> A separate retrospective analysis of 248 patients with biochemical recurrence demonstrated similar findings, with 89.5% of patients being found to have radiotracer-avid sites of disease.<sup>133</sup> In addition to those larger studies, case reports have been published demonstrating the ability of  $^{68}\text{Ga}$ -PSMA to detect a brain metastasis due to prostate cancer,<sup>134</sup> to be used with MR imaging for the detection of primary disease,<sup>135, 136</sup> and to evaluate the response of bone metastases to  $^{223}\text{Ra}$  therapy.<sup>137</sup> Although both  $^{18}\text{F}$ - and  $^{68}\text{Ga}$ -labeled small-molecule radiotracers for PSMA have demonstrated excellent promise, a recent manuscript by Dietlein *et al.* suggested that small lesions in patients with biochemical recurrence may be evaluated with higher fidelity by [ $^{18}\text{F}$ ] DCFpyL than by  $^{68}\text{Ga}$ -PSMA.<sup>138</sup>

## PSMA-targeted therapy and theranostic agents in human prostate cancer

Targeting of PSMA for prostate cancer therapy has been investigated using antibodies, minibodies, antibody-drug conjugates (ADCs), and small molecules. We will briefly discuss the former agents and then focus on small-molecule agents.

### Antibody-based therapies

Antibody therapy targeting PSMA was initiated using radiolabeled capromab pendetide (CYT-356) in two phase I dose-escalation studies, one in patients with metastatic castration-resistant prostate cancer and the other in patients with biochemical recurrence.<sup>139, 140</sup> In patients treated with <sup>90</sup>Y-labeled CYT-356, however, efficacy was lacking as antibody was unable to bind to viable tumor cells, and patients experienced dose-limiting myelosuppression. Subsequent clinical trials have investigated the deimmunized IgG monoclonal antibody, J591, previously radiolabeled with <sup>111</sup>In, <sup>90</sup>Y, and <sup>177</sup>Lu through a DOTA chelator. Patients that underwent trials with <sup>90</sup>Y- or <sup>177</sup>Lu-labeled J591 experienced reversible myelosuppression at higher doses.<sup>121, 141</sup> Radiographic tumor response and significant prostate-specific antigen (PSA) decline were observed only in patients receiving <sup>177</sup>Lu-labeled J591. Based on those results, a phase II trial in metastatic castration-resistant prostate cancer was initiated at two centers, with an initial cohort receiving 65 mCi/m<sup>2</sup> and a second cohort receiving 70 mCi/m<sup>2</sup>. Imaging studies revealed excellent targeting (94% of patients) and PSA declines were significant and greater in the higher dose cohort (71% vs. 46%), with thrombocytopenia as the most common severe hematologic toxicity and no significant non-hematologic toxicities.<sup>142</sup> A subsequent phase I trial of fractionated-dose <sup>177</sup>Lu-labeled J591 demonstrated improved tolerability.<sup>143</sup> Phase I trials using fractionated <sup>177</sup>Lu-J591 for radioimmunotherapy plus docetaxel as a radiosensitizer are ongoing [NCT00916123].

A significant drawback of antibodies for therapy is that full antibodies do not homogeneously penetrate tumors, resulting in diminished therapeutic potential. Therefore, Watanabe *et al.* developed an approach using antibody fragments such as small bivalent antibody fragments, or minibodies.<sup>144</sup> In a preclinical study they found that NIR photoimmunotherapy could be effected at an earlier time point after administration of the PSMA-targeted minibody relative to the intact antibody. Such studies further underscore the importance of pharmacokinetic optimization of PSMA-targeted agents to enable practical clinical implementation.

Another antibody-mediated approach has been to engineer J591 to interact with human immune effector cells to trigger antibody-dependent cell-mediated cytotoxicity (ADCC). In a dose-escalation trial in patients with progressive castration-resistant prostate cancer, dose correlated with degree of ADCC induction, with one patient who received 100 mg of J591 experiencing a reduction in PSA of greater than 50%.<sup>145</sup> In a phase II trial combining IL-2 (known to promote immune responses) and J591, there was a trend toward less progression in patients demonstrating natural killer cell expansion.<sup>146</sup>

## Antibody-drug conjugate therapies

Significant interest has surrounded enhancing the efficacy and/or reducing the toxicities of cytotoxic chemotherapies by using PSMA-targeted ADCs or nanoparticles. A pre-clinical study that employed a polymeric nanoparticle targeting PSMA containing the chemotherapeutic agent docetaxel (DTXL-TNP) showed enhanced tumor accumulation at 12 hours and prolonged tumor growth delay compared to solvent-based DTXL.<sup>147</sup> Preliminary reports of an ongoing phase I study in patients with advanced or metastatic solid cancers showed tumor shrinkage with DTXL-TNP at doses lower than solvent-based DTXL.<sup>147</sup> MLN2704, an ADC created by conjugating J591 to the anti-microtubule drug maytansinoid-1, was evaluated in a phase I study after demonstrating preclinical activity.<sup>148, 149</sup> Although a subsequent phase I/II study demonstrated limited efficacy with significant neurotoxicity using MLN2704, the trial established the potential of PSMA-targeted ADCs.<sup>150</sup> As a result, an additional PSMA-based ADC directing enzyme-activated cytotoxin release, and another delivering the toxin monomethylauristatin E (MMAE), are undergoing phase I and II investigations, respectively.<sup>151, 152</sup>

## Small molecule therapies

Recent studies have demonstrated the potential for clinical translation of PSMA-targeted small-molecule radiopharmaceutical therapies, as well as theranostic approaches combining targeted imaging and targeted therapy. Structures of recently reported <sup>68</sup>Ga/<sup>177</sup>Lu-based PSMA-targeting theranostic radiometals are shown in Table III, entries 2–15. Weineisen and coworkers recently evaluated three compounds,<sup>153, 154</sup> in which, the DOTA-monamide chelating agent (Table III, Entry 2) was replaced by 1,4,7,10-tetraazacyclododecane-1-(glutaric acid)-4,7,10-triacetic acid (DOTAGA), while maintaining the same Glu-Lys urea PSMA-targeting construct. The authors reported that due to metabolic instability of the L-amino acid residues on the linker, D-amino acids were implemented to provide metabolically stable agents. [<sup>68</sup>Ga]DOTAGA-ffk(Sub-KuE) (Table III, Entry 11) displayed favorable pharmacokinetics and high tumor accumulation in PSMA+ LNCaP tumor-bearing mice.<sup>153</sup> Further modification of the linker, specifically, replacing one D-Phe residue with lipophilic 4-iodo-D-tyrosine, resulted in [<sup>68</sup>Ga]DOTAGA-(Iy)fk(Sub-KuE), *i.e.*, PSMA I&T (Table III, Entry 12), which was recently evaluated both in a murine model and in initial proof-of-concept clinical studies.<sup>153</sup> Baum *et al.* have used a <sup>177</sup>Lu-labeled version of PSMA I&T in 60 patients with significant decreases in PSA observed and without demonstrable side effects. One patient experienced a decrease in PSA from 36 ng/mL to <1 ng/mL after three cycles of therapy (Figure 8) (Richard Baum, personal communication). The compounds of Table III, Entries 13 and 14, prepared by using CHX-A'-DTPA and DO3A, respectively, employed the Glu-Glu urea as the targeting moiety.<sup>155, 156</sup>

The radiohalogenated agent [<sup>131</sup>I]MIP-1095 (Table I, Entry 8) has been investigated in 28 patients with metastatic castration-resistant prostate cancer. After receiving a single cycle of [<sup>131</sup>I]MIP-1095 PSA values decreased by >50% in 61% of the men treated, with transient dry mouth as the most notable side-effect (in 25% of patients). With that treatment, involved lymph nodes and bone metastases received an estimated dose of more than 300 Gy of targeted radiation therapy.<sup>72</sup> Furthermore, the Auger electron emitter <sup>125</sup>I has been conjugated to urea-based DCIBzL (Table I, Entry 5) and has recently been shown to yield

significant antitumor efficacy in mice bearing PSMA+PC3 PIP xenografts, emphasizing the importance of PSMA internalization and perinuclear localization, as Auger electrons are known to have a very short range of <10  $\mu\text{m}$ .<sup>157</sup>

### Preclinical theranostics

Many of the translational theranostic agents targeting PSMA that employ radiometals use a strategy similar to that depicted in Figure 4 where the linker has been modified with various hydrophobic aromatic species in order to enhance affinity as first reported by Kularatne *et al.*<sup>75</sup> With respect to possible theranostics, Banerjee *et al.* have explored the positron emitting radiometal <sup>86</sup>Y ( $T_{1/2}$ =14.7 h) as an imaging radionuclide for PSMA, as agents incorporating it can be used for dosimetry estimates of the corresponding pure  $\beta$ -particle emitter, <sup>90</sup>Y, and possibly for modeling compounds that incorporate <sup>177</sup>Lu, which also uses the DOTA chelator. Structures are presented in Table III, Entries 4 and 7. Compound [<sup>86</sup>Y]6 (Table IV, Entry 7) was generated using the *p*-Bn-SCN-DOTA chelator and a diaminobutane linker, and provided the desired lower kidney uptake and higher tumor retention than other agents in this series,<sup>158</sup> making this agent particularly attractive for radiotherapy.

More complex PSMA-targeted theranostic agents, namely, those that do not solely leverage radionuclide therapy, have so far not been translated to the clinic. Chen *et al.* published a series of proof-of-principle experiments showing the versatility of a theranostic nanoplex.<sup>159</sup> The nanoplex contained three covalently linked components: 1) a pro-drug-activating enzyme bacterial cytosine deaminase (which converts a nontoxic pro-drug to the cytotoxic 5-fluorouracil); 2) an imaging reporter carrier poly-L-lysine labeled with the NIRF probe Cy 5.5; and 3) a vector for siRNA delivery to down-regulate choline kinase (which may enhance the effect of 5-FU). The nanoplex was radiolabeled with [<sup>111</sup>In] DOTA for SPECT imaging and targeted to PSMA through a low-molecular-weight, urea-based moiety. That strategy can be extended to other targets and types of cancer, increasing the precision of drug delivery to enhance the impact and safety of therapy, the chief goals of nanomedicine.

### PSMA as a target for imaging and therapy in other cancers

PSMA expression in renal tubules, duodenal and colonic mucosa, and brain has been well defined.<sup>160</sup> PSMA expression on neovascular endothelial cells in a variety of solid tumors is likewise known, as indicated above. Literature on PSMA over-expression in non-prostate prostate tumor epithelial cells is beginning to emerge. In this section, we will discuss PSMA over-expression in epithelial and endothelial cells of non-prostate tumors and provide an update on its use for imaging and therapy in this context.

In one of the earliest observations, Silver *et al.* reported intense PSMA staining in the endothelial cells of capillary vessels in peritumoral and endotumoral areas of renal and colon carcinomas.<sup>12</sup> Further confirmatory studies to detect PSMA expression in neovasculature were later carried out by Chang *et al.*, in benign tissues, prostate and 15 types of non-prostate tumors using five different PSMA monoclonal antibodies. Those studies showed strong PSMA immunoreactivity in the neovasculature of a variety of tumors including renal cell carcinoma (RCC), glioblastoma (GBM), melanoma and non-small cell lung cancer.<sup>32</sup> No staining was observed in the epithelial cells of non-prostate tumors. Although tumor

epithelial cells were universally positive for PSMA, interestingly only a fraction of the corresponding tumors showed PSMA immunoreactivity in the neovasculature.<sup>32</sup> Those immunohistochemical observations were confirmed using RT-PCR and *in situ* hybridization studies in different tumor types by the same group.<sup>31</sup>

PSMA expression is well characterized in the neovasculature of renal neoplasms. Nearly 76% of clear cell RCC and 31% of chromophobe RCC were shown to be positive for PSMA.<sup>161</sup> PSMA expression in RCC may become important for this cancer with few diagnostic imaging options. Also, PSMA expression was detected in 66% of gastric and 85% of colorectal carcinomas tested.<sup>34</sup> Similarly, PSMA expression in neovasculature from GBM was demonstrated to a variable extent in 100% of specimens tested.<sup>162</sup> Results from other groups confirmed those observations,<sup>163</sup> suggesting a new role for PSMA-targeted imaging and therapeutics in management of GBM. PSMA expression was shown to be associated with poor survival outcome for several non-prostate tumor types. Detection of PSMA within neovasculature in nearly 50% of oral squamous cell carcinoma specimens tested was associated with reduced survival.<sup>164</sup> Similarly, 46% of osteosarcoma specimens showed PSMA immunoreactivity in the neovasculature that correlated with poor survival.<sup>165</sup> In a recent study by Wernicke and coworkers, 74% of the primary breast cancers tested showed PSMA immunoreactivity in the neovasculature.<sup>166</sup> High PSMA expression in the neovasculature on breast cancers was shown to result in reduced overall survival.

In addition to primary tumors, PSMA expression was also detected in the neovasculature of metastatic lesions. Metastatic tissue from RCC showed consistent PSMA expression in the neovasculature.<sup>33</sup> Also, nearly 80% of liver and colon carcinoma metastases tested were positive for PSMA in the neovasculature.<sup>167</sup> Similarly, 100% of brain metastases due to breast cancer showed PSMA immunoreactivity in the neovasculature.<sup>166</sup> Availability of PSMA-targeted antibodies and their detailed characterization has improved the detection of PSMA in the epithelial cells of non-prostate tumors. PSMA expression in lung cancer cells was recently reported. Nearly 54% of lung tumor cells and 85% of lung tumor endothelial cells demonstrated PSMA immunoreactivity.<sup>168</sup> Although PSMA expression in non-prostate tumor epithelial cells and endothelium is gaining traction, and case reports are appearing, its diagnostic and therapeutic value in non-prostate cancer has yet to be established.

In a recent study, Pandit-Taskar *et al.* investigated the use of <sup>111</sup>In-labeled J591 for imaging a variety of solid tumors, demonstrating that 74% of skeletal lesions, 53% of lymph node lesions, and 64% of other visceral lesions were identified by the antibody, with uptake seen in lesions from all investigated tumor types.<sup>169</sup> Also, Demirci *et al.* imaged a patient with known metastatic ccRCC using <sup>68</sup>Ga-PSMA PET/CT.<sup>170</sup> The authors observed multiple sites of metastatic disease that were occult with FDG PET/CT. Rowe *et al.* have similarly observed metastases due to ccRCC using [<sup>18</sup>F]DCFPyL (unpublished results). Comparison with FDG PET/CT indicated higher standardized uptake values for the PSMA-targeted agent in this tumor that is typically difficult to detect with FDG (Figure 9). Those results are important due to the often small and unusual sites of metastasis seen with ccRCC that point to a potential increase in diagnostic yield with PSMA-based imaging, as well as the possibility of evaluating response to therapy given the anti-angiogenic action of many of the chemotherapeutic options for metastatic ccRCC (*e.g.* various tyrosine kinase inhibitors).

## Conclusions

Dedicated work over the last decade in medicinal chemistry has provided a number of small-molecule SPECT and PET ligands for *in vivo* imaging of PSMA, as well as theranostic and therapeutic agents. A number of those agents have now been translated and clinically evaluated in patients with prostate cancer, and specific and appropriate indications for their application are emerging. Given the higher sensitivity and specificity of PSMA-based PET in the detection of metastatic prostate cancer relative to contrast enhanced CT and bone scan, it seems that these agents will be well suited for the evaluation of patients with early biochemical recurrence. Indeed, in such patients the ability to identify recurrent metastatic disease within the pelvis as opposed to disease at more distant sites would allow for selection of appropriate therapy, such as salvage pelvic radiotherapy *versus* systemic androgen deprivation therapy. The use of PSMA imaging agents for upfront staging of patients with high-risk disease may allow for detection of unsuspected sites of lymph node or bone metastases, again guiding selection of therapy. In those patients with low-risk, organ-confined disease, early data suggest that uptake of PSMA-targeted agents may correlate with the aggressiveness of the primary tumor, which may aid in selection of patients who should undergo surgery or radiotherapy versus active surveillance.

Emerging data suggest that radiolabeled compounds targeting PSMA may prove to be effective theranostic and therapeutic options for patients with metastatic prostate cancer. Promising early clinical studies with  $^{68}\text{Ga}/^{177}\text{Lu}$ -based PSMA-targeting radiometals have demonstrated tumor responses with surprisingly little toxicity. Such compounds may find an important role in treatment, particularly in patients whose tumors have become castration-resistant but retain PSMA expression. Furthermore, the expression of PSMA in the neovasculature of numerous non-prostate solid tumors coupled with recent reports of successful PSMA-based PET/CT imaging of such cancers support the concept that PSMA-targeted imaging and therapy can be extended beyond management of prostate cancer.

## Acknowledgments

*Funding.* CA134675, CA184228, CA183031

## References

1. Akhurst T, MacManus M, Hicks RJ. Lung cancer. PET clinics. 2015; 10:147–58. [PubMed: 25829084]
2. Meignan M, Itti E, Gallamini A, Younes A. FDG PET/CT imaging as a biomarker in lymphoma. Eur J Nucl Med Mol Imaging. 2015; 42:623–33. [PubMed: 25573631]
3. Schmidt T, Lordick F, Herrmann K, Ott K. Value of functional imaging by PET in esophageal cancer. J Natl Compr Canc Netw. 2015; 13:239–47. [PubMed: 25691614]
4. Wahl RL, Jacene H, Kasamon Y, Lodge MA. From RECIST to PERCIST: Evolving Considerations for PET response criteria in solid tumors. J Nucl Med. 2009; 50(Suppl 1):122s–50s. [PubMed: 19403881]
5. Fanti S, Nanni C, Ambrosini V, Gross MD, Rubello D, Farsad M. PET in genitourinary tract cancers. Q J Nucl Med Mol Imaging. 2007; 51:260–71. [PubMed: 17464269]
6. Kumar R, Zhuang H, Alavi A. PET in the management of urologic malignancies. Radiol Clin North Am. 2004; 42:1141–53. ix. [PubMed: 15488563]



7. Takahashi N, Inoue T, Lee J, Yamaguchi T, Shizukuishi K. The roles of PET and PET/CT in the diagnosis and management of prostate cancer. *Oncology*. 2007; 72:226–33. [PubMed: 18176088]
8. Alonzi R, Padhani AR, Allen C. Dynamic contrast enhanced MRI in prostate cancer. *Eur J Radiol*. 2007; 63:335–50. [PubMed: 17689907]
9. Barinka C, Rojas C, Slusher B, Pomper M. Glutamate carboxypeptidase II in diagnosis and treatment of neurologic disorders and prostate cancer. *Curr Med Chem*. 2012; 19:856–70. [PubMed: 22214450]
10. Ben Jemaa A, Bouraoui Y, Sallami S, Banasr A, Nouria Y, Horchani A, et al. Cellular distribution and heterogeneity of Psa and PsmA expression in normal, hyperplasia and human prostate cancer. *Tunis Med*. 2013; 91:458–63. [PubMed: 24008878]
11. Zhang S, Zhang HS, Reuter VE, Slovin SF, Scher HI, Livingston PO. Expression of potential target antigens for immunotherapy on primary and metastatic prostate cancers. *Clin Cancer Res*. 1998; 4:295–302. [PubMed: 9516914]
12. Silver DA, Pellicer I, Fair WR, Heston WD, Cordon-Cardo C. Prostate-specific membrane antigen expression in normal and malignant human tissues. *Clin Cancer Res*. 1997; 3:81–5. [PubMed: 9815541]
13. Santoni M, Scarpelli M, Mazzucchelli R, Lopez-Beltran A, Cheng L, Cascinu S, et al. Targeting prostate-specific membrane antigen for personalized therapies in prostate cancer: morphologic and molecular backgrounds and future promises. *J Biol Regul Homeost Agents*. 2014; 28:555–63. [PubMed: 25620167]
14. Ross JS, Sheehan CE, Fisher HAG, Kaufman RP, Kaur P, Gray K, et al. Correlation of primary tumor prostate-specific membrane antigen expression with disease recurrence in prostate cancer. *Clin Cancer Res*. 2003; 9:6357–62. [PubMed: 14695135]
15. Schmidt B, Anastasiadis AG, Seifert HH, Franke KH, Oya M, Ackermann R. Detection of circulating prostate cells during radical prostatectomy by standardized PSMA RT-PCR: association with positive lymph nodes and high malignant grade. *Anticancer Res*. 2003; 23:3991–9. [PubMed: 14666708]
16. Barwe SP, Maul RS, Christiansen JJ, Anilkumar G, Cooper CR, Kohn DB, et al. Preferential association of prostate cancer cells expressing prostate specific membrane antigen to bone marrow matrix. *Int J Oncol*. 2007; 30:899–904. [PubMed: 17332929]
17. Douglas TH, Connelly RR, McLeod DG, Erickson SJ, Barren R 3rd, Murphy GP. Effect of exogenous testosterone replacement on prostate-specific antigen and prostate-specific membrane antigen levels in hypogonadal men. *J Surg Oncol*. 1995; 59:246–50. [PubMed: 7543173]
18. Denmeade SR, Sokoll LJ, Dalrymple S, Rosen DM, Gady AM, Bruzek D, et al. Dissociation between androgen responsiveness for malignant growth vs. expression of prostate specific differentiation markers PSA, hK2, and PSMA in human prostate cancer models. *Prostate*. 2003; 54:249–57. [PubMed: 12539223]
19. Bacich DJ, Pinto JT, Tong WP, Heston WD. Cloning, expression, genomic localization, and enzymatic activities of the mouse homolog of prostate-specific membrane antigen/NAALADase/folate hydrolase. *Mamm Genome*. 2001; 12:117–23. [PubMed: 11210180]
20. Wang X, Ma D, Olson WC, Heston WD. In vitro and in vivo responses of advanced prostate tumors to PSMA ADC, an auristatin-conjugated antibody to prostate-specific membrane antigen. *Mol Cancer Ther*. 2011; 10:1728–39. [PubMed: 21750220]
21. Ghosh A, Heston WD. Effect of carbohydrate moieties on the folate hydrolysis activity of the prostate specific membrane antigen. *Prostate*. 2003; 57:140–51. [PubMed: 12949938]
22. Barinka C, Sacha P, Sklenar J, Man P, Bezouska K, Slusher BS, et al. Identification of the N-glycosylation sites on glutamate carboxypeptidase II necessary for proteolytic activity. *Protein Sci*. 2004; 13:1627–35. [PubMed: 15152093]
23. Schulke N, Varlamova OA, Donovan GP, Ma D, Gardner JP, Morrissey DM, et al. The homodimer of prostate-specific membrane antigen is a functional target for cancer therapy. *Proc Natl Acad Sci U S A*. 2003; 100:12590–5. [PubMed: 14583590]
24. Kovar JL, Cheung LL, Simpson MA, Olive DM. Pharmacokinetic and Biodistribution assessment of a near infrared-labeled psma-specific small molecule in tumor-bearing mice. *Prostate Cancer*. 2014; 2014:104248. [PubMed: 24804103]

25. Barua S, Rege K. The influence of mediators of intracellular trafficking on transgene expression efficacy of polymer-plasmid DNA complexes. *Biomaterials*. 2010; 31:5894–902. [PubMed: 20452664]
26. Yao V, Berkman CE, Choi JK, O'Keefe DS, Bacich DJ. Expression of prostate-specific membrane antigen (PSMA), increases cell folate uptake and proliferation and suggests a novel role for PSMA in the uptake of the non-polyglutamated folate, folic acid. *Prostate*. 2010; 70:305–16. [PubMed: 19830782]
27. Yao V, Parwani A, Maier C, Heston WD, Bacich DJ. Moderate expression of prostate-specific membrane antigen, a tissue differentiation antigen and folate hydrolase, facilitates prostate carcinogenesis. *Cancer Res*. 2008; 68:9070–7. [PubMed: 18974153]
28. Luthi-Carter R, Barczak AK, Speno H, Coyle JT. Molecular characterization of human brain N-acetylated alpha-linked acidic dipeptidase (NAALADase). *J Pharmacol Exp Ther*. 1998; 286:1020–5. [PubMed: 9694964]
29. O'Keefe DS, Su SL, Bacich DJ, Horiguchi Y, Luo Y, Powell CT, et al. Mapping, genomic organization and promoter analysis of the human prostate-specific membrane antigen gene. *Biochim Biophys Acta*. 1998; 1443:113–27. [PubMed: 9838072]
30. Trover JK, Beckett ML, Wright GL. Detection and characterization of the prostate specific membrane antigen (PSMA) in tissue extracts and body fluids. *Int J Cancer*. 1995; 62:552–8. [PubMed: 7665226]
31. Chang SS, O'Keefe DS, Bacich DJ, Reuter VE, Heston WD, Gaudin PB. Prostate-specific membrane antigen is produced in tumor-associated neovasculature. *Clin Cancer Res*. 1999; 5:2674–81. [PubMed: 10537328]
32. Chang SS, Reuter VE, Heston WD, Bander NH, Grauer LS, Gaudin PB. Five different anti-prostate-specific membrane antigen (PSMA) antibodies confirm PSMA expression in tumor-associated neovasculature. *Cancer Res*. 1999; 59:3192–8. [PubMed: 10397265]
33. Chang SS, Reuter VE, Heston WD, Gaudin PB. Metastatic renal cell carcinoma neovasculature expresses prostate-specific membrane antigen. *Urology*. 2001; 57:801–5. [PubMed: 11306418]
34. Haffner MC, Kronberger IE, Ross JS, Sheehan CE, Zitt M, Muhlmann G, et al. Prostate-specific membrane antigen expression in the neovasculature of gastric and colorectal cancers. *Hum Pathol*. 2009; 40:1754–61. [PubMed: 19716160]
35. Zhou J, Neale JH, Pomper MG, Kozikowski AP. NAAG peptidase inhibitors and their potential for diagnosis and therapy. *Nat Rev Drug Discov*. 2005; 4:1015–26. [PubMed: 16341066]
36. Byun, YM.; Lupold, S.; Pomper, MG. Drug design of zinc-enzyme inhibitors. In: Superan, JY., editor. Recent development of diagnostic and therapeutic agents targeting glutamate carboxypeptidase II (GCPII). Hoboken, NJ: Wiley; 2009.
37. Jackson PF, Cole DC, Slusher BS, Stetz SL, Ross LE, Donzanti BA, et al. Design, synthesis, and biological activity of a potent inhibitor of the neuropeptidase N-acetylated alpha-linked acidic dipeptidase. *J Med Chem*. 1996; 39:619–22. [PubMed: 8558536]
38. Slusher BS, Vornov JJ, Thomas AG, Hurn PD, Harukuni I, Bhardwaj A, et al. Selective inhibition of NAALADase, which converts NAAG to glutamate, reduces ischemic brain injury. *Nat Med*. 1999; 5:1396–402. [PubMed: 10581082]
39. Anderson MO, Wu LY, Santiago NM, Moser JM, Rowley JA, Bolstad ES, et al. Substrate specificity of prostate-specific membrane antigen. *Bioorg Med Chem*. 2007; 15:6678–86. [PubMed: 17764959]
40. Liu T, Wu LY, Kazak M, Berkman CE. Cell-Surface labeling and internalization by a fluorescent inhibitor of prostate-specific membrane antigen. *Prostate*. 2008; 68:955–64. [PubMed: 18361407]
41. Maung J, Mallari JP, Girtsman TA, Wu LY, Rowley JA, Santiago NM, et al. Probing for a hydrophobic a binding register in prostate-specific membrane antigen with phenylalkylphosphonamidates. *Bioorg Med Chem*. 2004; 12:4969–79. [PubMed: 15336276]
42. Kozikowski AP, Nan F, Conti P, Zhang J, Ramadan E, Bzdega T, et al. Design of remarkably simple, yet potent urea-based inhibitors of glutamate carboxypeptidase II (NAALADase). *J Med Chem*. 2001; 44:298–301. [PubMed: 11462970]

43. Kozikowski AP, Zhang J, Nan F, Petukhov PA, Grajkowska E, Wroblewski JT, et al. Synthesis of urea-based inhibitors as active site probes of glutamate carboxypeptidase II: efficacy as analgesic agents. *J Med Chem.* 2004; 47:1729–38. [PubMed: 15027864]
44. Pavlicek J, Ptacek J, Barinka C. Glutamate Carboxypeptidase II: An Overview of Structural Studies and Their Importance for Structure-Based Drug Design and Deciphering the Reaction Mechanism of the Enzyme. *Curr Med Chem.* 2012; 19:1300–9. [PubMed: 22304708]
45. Barinka C, Byun Y, Dusich CL, Banerjee SR, Chen Y, Castanares M, et al. Interactions between human glutamate carboxypeptidase II and urea-based inhibitors: structural characterization. *J Med Chem.* 2008; 51:7737–43. [PubMed: 19053759]
46. Chen Y, Foss CA, Byun Y, Nimmagadda S, Pullambhatla M, Fox JJ, et al. Radiohalogenated prostate-specific membrane antigen (PSMA)-based ureas as imaging agents for prostate cancer. *J Med Chem.* 2008; 51:7933–43. [PubMed: 19053825]
47. Tykvar J, Schimer J, Barinkova J, Pacht P, Postova-Slavetinska L, Majer P, et al. Rational design of urea-based glutamate carboxypeptidase II (GCPII) inhibitors as versatile tools for specific drug targeting and delivery. *Bioorg Med Chem.* 2014; 22:4099–108. [PubMed: 24954515]
48. Tykvar J, Schimer J, Jancarik A, Barinkova J, Navratil V, Starkova J, et al. Design of Highly Potent Urea-Based, Exosite-Binding Inhibitors Selective for Glutamate Carboxypeptidase II. *J Med Chem.* 2015; 58:4357–63. [PubMed: 25923815]
49. Wang H, Byun Y, Barinka C, Pullambhatla M, Bhang HE, Fox JJ, et al. Bioisosterism of urea-based GCPII inhibitors: Synthesis and structure-activity relationship studies. *Bioorg Med Chem Lett.* 2010; 20:392–7. [PubMed: 19897367]
50. Zhang AX, Murelli RP, Barinka C, Michel J, Cocleaza A, Jorgensen WL, et al. A remote arene-binding site on prostate specific membrane antigen revealed by antibody-recruiting small molecules. *J Am Chem Soc.* 2010; 132:12711–6. [PubMed: 20726553]
51. Pomper MG, Musachio JL, Zhang J, Scheffel U, Zhou Y, Hilton J, et al. 11C-MCG: synthesis, uptake selectivity, and primate PET of a probe for glutamate carboxypeptidase II (NAALADase). *Mol Imaging.* 2002; 1:96–101. [PubMed: 12920850]
52. Foss CA, Mease RC, Fan H, Wang Y, Ravert HT, Dannals RF, et al. Radiolabeled small-molecule ligands for prostate-specific membrane antigen: in vivo imaging in experimental models of prostate cancer. *Clin Cancer Res.* 2005; 11:4022–8. [PubMed: 15930336]
53. Mease RC, Dusich CL, Foss CA, Ravert HT, Dannals RF, Seidel J, et al. N-[N-[(S)-1,3-Dicarboxypropyl]carbamoyl]-4-[18F] fluorobenzyl-L-cysteine, [18F]DCFBC: a new imaging probe for prostate cancer. *Clin Cancer Res.* 2008; 14:3036–43. [PubMed: 18483369]
54. Chen Y, Pullambhatla M, Foss CA, Byun Y, Nimmagadda S, Senthamizhchelvan S, et al. 2-(3-(1-Carboxy-5-[(6-[18F]fluoro-pyridine-3-carbonyl)-amino]-pentyl)-ureido)-pentanedioic acid, [18F]DCFPyL, a PSMA-based PET imaging agent for prostate cancer. *Clin Cancer Res.* 2011; 17:7645–53. [PubMed: 22042970]
55. Pomper, MG.; Mease, RC.; Chen, Y., inventors. WO. 2010/014933 A2. 2010. PSMA-binding agents and uses thereof
56. Hooshyar Yousefi, B.; Bollinger, M.; Kessler, H.; Wester, H-J., inventors. WO. 2015/004029 A1 . 2015. <sup>18</sup>F-Labeling of aromatic and heteroaromatic molecules with unprotected carboxylic acid groups
57. Malik N, Machulla HJ, Solbach C, Winter G, Reske SN, Zlatopolskiy B. Radiosynthesis of a new PSMA targeting ligand ([18F] FPy-DUPA-Pep). *Appl Radiat Isot.* 2011; 69:1014–8. [PubMed: 21498081]
58. Huang SS, Wang X, Zhang Y, Doke A, DiFilippo FP, Heston WD. Improving the biodistribution of PSMA-targeting tracers with a highly negatively charged linker. *Prostate.* 2014; 74:702–13. [PubMed: 24615708]
59. Malik N, Zlatopolsky B, Machulla H-J, Reske SN, Solbach C. One pot radiofluorination of a new potential PSMA ligand {Al<sup>18</sup>F} NOTA-DUPA-Pep. *J Label Compd Radiopharm.* 2012; 55:320–5.
60. Malik N, Baur B, Winter G, Reske SN, Beer AJ, Solbach C. Radiofluorination of PSMA-HBED via AlF chelation and biological evaluations in vitro. *Mol Imaging Biol.* 2015 Epub ahead of print.
61. Al-Momani E, Malik N, Machulla H-J, Reske SN, Solbach C. Radiosynthesis of [18f]FET-Try-urea-glu ([18F]FETUG) as a new PSMA ligand. *J Radioanal Nucl Chemistry.* 2013; 295:2289–94.

62. Wang, E.; Kolb, H.; Szardenings, AK.; Liu, C.; Walsh, JC.; Chen, G., et al., inventors. WO. 2013028664 A1. 2013. Preparation of glutamic acid-based peptidomimetic protate-specific membrane antigen PSMA binding agents for imaging use
63. Walsh J, Mu F. Synthesis and preclinical validation of [<sup>18</sup>F]P238 as a PET imaging agent for prostate specific membrane antigen (PSMA). *Abstract J Nucl Med.* 2015; 56(Suppl 3):65.
64. Lapi SE, Wahnische H, Pham D, Wu LY, Nedrow-Byers JR, Liu T, et al. Assessment of an <sup>18</sup>F-labeled phosphoramidate peptidomimetic as a new prostate-specific membrane antigen-targeted imaging agent for prostate cancer. *J Nucl Med.* 2009; 50:2042–8. [PubMed: 19910433]
65. Ley CR, Beattie NR, Dannoon S, Regan M, VanBrocklin H, Berkman CE. Synthesis and evaluation of constrained phosphoramidate inhibitors of prostate-specific membrane antigen. *Bioorg Med Chem Lett.* 2015; 25:2536–9. [PubMed: 25956413]
66. Graham K, Lesche R, Gromov AV, Bohnke N, Schafer M, Hassfeld J, et al. Radiofluorinated derivatives of 2-(phosphonomethyl)pentanedioic acid as inhibitors of prostate specific membrane antigen (PSMA) for the imaging of prostate cancer. *J Med Chem.* 2012; 55:9510–20. [PubMed: 23025786]
67. Lesche R, Ketschau G, Gromov AV, Bohnke N, Borkowski S, Monning U, et al. Preclinical evaluation of BAY 1075553, a novel (<sup>18</sup>F)-labelled inhibitor of prostate-specific membrane antigen for PET imaging of prostate cancer. *Eur J Nucl Med Mol Imaging.* 2014; 41:89–101. [PubMed: 23955632]
68. Hillier SM, Maresca KP, Femia FJ, Marquis JC, Foss CA, Nguyen N, et al. Preclinical evaluation of novel glutamate-urea-lysine analogues that target prostate-specific membrane antigen as molecular imaging pharmaceuticals for prostate cancer. *Cancer Res.* 2009; 69:6932–40. [PubMed: 19706750]
69. Maresca KP, Hillier SM, Femia FJ, Keith D, Barone C, Joyal JL, et al. A series of halogenated heterodimeric inhibitors of prostate specific membrane antigen (PSMA) as radiolabeled probes for targeting prostate cancer. *J Med Chem.* 2009; 52:347–57. [PubMed: 19111054]
70. Darwish A, Blacker M, Janzen N, Rathmann SM, Czorny S, Hillier SM, et al. Triazole Appending Agent (TAAG): A New Synthon for Preparing Iodine-Based Molecular Imaging and Radiotherapy Agents. *ACS Med Chem Lett.* 2012; 3:313–6. [PubMed: 24900470]
71. Barrett JA, Coleman RE, Goldsmith SJ, Vallabhajosula S, Petry NA, Cho S, et al. First-in-man evaluation of 2 high-affinity PSMA-avid small molecules for imaging prostate cancer. *J Nucl Med.* 2013; 54:380–7. [PubMed: 23303962]
72. Zechmann CM, Afshar-Oromieh A, Armor T, Stubbs JB, Mier W, Hadaschik B, et al. Radiation dosimetry and first therapy results with a (<sup>124</sup>I)/ (<sup>131</sup>I)-labeled small molecule (MIP-1095) targeting PSMA for prostate cancer therapy. *Eur J Nucl Med Mol Imaging.* 2014; 41:1280–92. [PubMed: 24577951]
73. Banerjee SR, Foss CA, Castanares M, Mease RC, Byun Y, Fox JJ, et al. Synthesis and evaluation of technetium-99m- and rhenium- labeled inhibitors of the prostate-specific membrane antigen (PSMA). *J Med Chemistry.* 2008; 51:4504–17.
74. Ray Banerjee S, Pullambhatla M, Foss CA, Falk A, Byun Y, Nimmagadda S, et al. Effect of chelators on the pharmacokinetics of (<sup>99m</sup>Tc)-labeled imaging agents for the prostate-specific membrane antigen (PSMA). *J Med Chem.* 2013; 56:6108–21. [PubMed: 23799782]
75. Kularatne SA, Zhou Z, Yang J, Post CB, Low PS. Design, synthesis, and preclinical evaluation of prostate-specific membrane antigen targeted (<sup>99m</sup>Tc)-radioimaging agents. *Mol Pharm.* 2009; 6:790–800. [PubMed: 19361232]
76. Maresca KP, Hillier SM, Lu G, Marquis JC, Zimmerman CN, Eckelman WC, et al. Small molecule inhibitors of PSMA incorporating technetium-99m for imaging prostate cancer: Effects of chelate design on pharmacokinetics. *Inorganica Chimica Acta.* 2012 Jul 1. 389:168–75.
77. Lu G, Maresca KP, Hillier SM, Zimmerman CN, Eckelman WC, Joyal JL, et al. Synthesis and SAR of (<sup>99m</sup>Tc)/Re-labeled small molecule prostate specific membrane antigen inhibitors with novel polar chelates. *Bioorg Med Chem Lett.* 2013; 23:1557–63. [PubMed: 23333070]
78. Hillier SM, Maresca KP, Lu G, Merkin RD, Marquis JC, Zimmerman CN, et al. <sup>99m</sup>Tc-labeled small-molecule inhibitors of prostate-specific membrane antigen for molecular imaging of prostate cancer. *J Nucl Med.* 2013; 54:1369–76. [PubMed: 23733925]

79. Nedrow-Byers JR, Moore AL, Ganguly T, Hopkins MR, Fulton MD, Benny PD, et al. PSMA-targeted SPECT agents: mode of binding effect on in vitro performance. *Prostate*. 2013; 73:355–62. [PubMed: 22911263]
80. Nedrow-Byers JR, Jabbes M, Jewett C, Ganguly T, He H, Liu T, et al. A phosphoramidate-based prostate-specific membrane antigen-targeted SPECT agent. *Prostate*. 2012; 72:904–12. [PubMed: 22670265]
81. Misra P, Humblet V, Pannier N, Maison W, Frangioni JV. Production of multimeric prostate-specific membrane antigen small-molecule radiotracers using a solid-phase <sup>99m</sup>Tc preloading strategy. *J Nucl Med*. 2007; 48:1379–89. [PubMed: 17631555]
82. Banerjee SR, Pullambhatla M, Byun Y, Nimmagadda S, Green G, Fox JJ, et al. <sup>68</sup>Ga-labeled inhibitors of prostate-specific membrane antigen (PSMA) for imaging prostate cancer. *J Med Chem*. 2010; 53:5333–41. [PubMed: 20568777]
83. Eder M, Schafer M, Bauder-Wust U, Hull WE, Wangler C, Mier W, et al. <sup>68</sup>Ga-complex lipophilicity and the targeting property of a urea-based PSMA inhibitor for PET imaging. *Bioconjug Chem*. 2012; 23:688–97. [PubMed: 22369515]
84. Martell AE, Motekaitis RJ, Clarke ET, Harrison JJ. Synthesis of N,N'-di(2-hydroxybenzyl)ethylenediamine-N,N'-diacetic acid (HBED) and derivatives. *Can J Chem*. 1986; 64:449–56.
85. Li Y, Martell AE, Hancock RD, Reibenspies JH, Anderson CJ, Welch MJ. N,N'-Ethylene-L-cysteine (EC) and Its Metal Complexes: Synthesis, Characterization, Crystal Structures, and Equilibrium Constants. *Inorg Chem*. 1996; 35:404–14. [PubMed: 11666222]
86. Sun Y, Anderson CJ, Pajeau TS, Reichert DE, Hancock RD, Motekaitis RJ, et al. Indium (III) and gallium (III) complexes of bis(aminoethanethiol) ligands with different denticities: stabilities, molecular modeling, and in vivo behavior. *J Med Chemistry*. 1996; 39:458–70.
87. Eder M, Wangler C, Knackmuss S, LeGall F, Little M, Haberkorn U, et al. Tetrafluorophenolate of HBED-CC: a versatile conjugation agent for <sup>68</sup>Ga-labeled small recombinant antibodies. *Eur J Nucl Med Mol Imaging*. 2008; 35:1878–86. [PubMed: 18509635]
88. Roesch F, Riss PJ. The renaissance of the (6)(8)Ge/(6)(8)Ga radionuclide generator initiates new developments in (6)(8)Ga radiopharmaceutical chemistry. *Curr Top Med Chem*. 2010; 10:1633–68. [PubMed: 20583984]
89. Banerjee SR, Chen Z, Pullambhatla M, Mease RC, Pomper MG. A Preclinical Comparative Study of <sup>68</sup>Ga-Labeled DOTA, NOTA and HBED-CC Chelated PSMA-targeted Radiotracers. *J Nucl Med*. 2015; 56:2A–30. abstract 64.
90. Benesova M, Schafer M, Bauder-Wust U, Afshar-Oromieh A, Kratochwil C, Mier W, et al. Preclinical evaluation of a tailor- Made DOTA-conjugated PSMA inhibitor with optimized linker moiety for imaging and endoradiotherapy of prostate cancer. *J Nucl Med*. 2015; 56:914–20. [PubMed: 25883127]
91. Eder M, Schafer M, Bauder-Wust U, Haberkorn U, Eisenhut M, Kopka K. Preclinical evaluation of a bispecific low-molecular heterodimer targeting both PSMA and GRPR for improved PET imaging and therapy of prostate cancer. *Prostate*. 2014; 74:659–68. [PubMed: 24464532]
92. Banerjee SR, Pullambhatla M, Foss CA, Nimmagadda S, Ferdani R, Anderson CJ, et al. (6)(4)Cu-labeled inhibitors of prostate-specific membrane antigen for PET imaging of prostate cancer. *J Med Chem*. 2014; 57:2657–69. [PubMed: 24533799]
93. Bandari RP, Jiang Z, Reynolds TS, Bernskoetter NE, Szczodroski AF, Bassuner KJ, et al. Synthesis and biological evaluation of copper-64 radiolabeled [DUPA-6-Ahx-(NODAGA)-5-Ava-BBN(7–14)NH<sub>2</sub>], a novel bivalent targeting vector having affinity for two distinct biomarkers (GRPr/PSMA) of prostate cancer. *Nucl Med Biol*. 2014; 41:355–63. [PubMed: 24508213]
94. Hao G, Kumar A, Dobin T, Oz OK, Hsieh JT, Sun X. A multivalent approach of imaging probe design to overcome an endogenous anion binding competition for noninvasive assessment of prostate specific membrane antigen. *Mol Pharm*. 2013; 10:2975–85. [PubMed: 23768233]
95. Baranyai Z, Reich D, Vagner A, Weineisen M, Toth I, Wester HJ, et al. A shortcut to high-affinity Ga-68 and Cu-64 radiopharmaceuticals: one-pot click chemistry trimerisation on the TRAP platform. *Dalton Trans*. 2015; 44:11137–46. [PubMed: 25999035]



96. Nguyen QT, Tsien RY. Fluorescence-guided surgery with live molecular navigation--a new cutting edge. *Nat Rev Cancer*. 2013; 13:653–62. [PubMed: 23924645]
97. Vahrmeijer AL, Hutteman M, van der Vorst JR, van de Velde CJ, Frangioni JV. Image-guided cancer surgery using near-infrared fluorescence. *Nat Rev Clin Oncol*. 2013; 10:507–18. [PubMed: 23881033]
98. Humblet V, Lapidus R, Williams LR, Tsukamoto T, Rojas C, Majer P, et al. High-affinity near-infrared fluorescent small-molecule contrast agents for in vivo imaging of prostate-specific membrane antigen. *Mol Imaging*. 2005; 4:448–62. [PubMed: 16285907]
99. Humblet V, Misra P, Bhushan KR, Nasr K, Ko YS, Tsukamoto T, et al. Multivalent scaffolds for affinity maturation of small molecule cell surface binders and their application to prostate tumor targeting. *J Med Chem*. 2009; 52:544–50. [PubMed: 19108655]
100. Liu T, Nedrow-Byers JR, Hopkins MR, Berkman CE. Spacer length effects on in vitro imaging and surface accessibility of fluorescent inhibitors of prostate specific membrane antigen. *Bioorg Med Chem Lett*. 2011; 21:7013–6. [PubMed: 22018464]
101. Liu T, Wu LY, Hopkins MR, Choi JK, Berkman CE. A targeted low molecular weight near-infrared fluorescent probe for prostate cancer. *Bioorg Med Chem Lett*. 2010; 20:7124–6. [PubMed: 20947349]
102. Chen Y, Dhara S, Banerjee SR, Byun Y, Pullambhatla M, Mease RC, et al. A low molecular weight PSMA-based fluorescent imaging agent for cancer. *Biochem Biophys Res Commun*. 2009; 390:624–9. [PubMed: 19818734]
103. Chen Y, Pullambhatla M, Banerjee SR, Byun Y, Stathis M, Rojas C, et al. Synthesis and biological evaluation of low molecular weight fluorescent imaging agents for the prostate-specific membrane antigen. *Bioconjug Chem*. 2012; 23:2377–85. [PubMed: 23157641]
104. Neuman BP, Eifler JB, Castanares M, Chowdhury WH, Chen Y, Mease RC, et al. Real-time, near-infrared fluorescence imaging with an optimized dye/light source/camera combination for surgical guidance of prostate cancer. *Clin Cancer Res*. 2015; 21:771–80. [PubMed: 25501577]
105. Kelderhouse LE, Chelvam V, Wayua C, Mahalingam S, Poh S, Kularatne SA, et al. Development of tumor-targeted near infrared probes for fluorescence guided surgery. *Bioconjug Chem*. 2013; 24:1075–80. [PubMed: 23642154]
106. Wang X, Huang SS, Heston WD, Guo H, Wang BC, Basilion JP. Development of targeted near-infrared imaging agents for prostate cancer. *Mol Cancer Ther*. 2014; 13:2595–606. [PubMed: 25239933]
107. Shallal HM, Minn I, Banerjee SR, Lisok A, Mease RC, Pomper MG. Heterobivalent agents targeting PSMA and integrin-alpha<sub>v</sub>beta<sub>3</sub>. *Bioconjugate Chemistry*. 2014; 25:393–405. [PubMed: 24410012]
108. Banerjee SR, Pullambhatla M, Shallal H, Lisok A, Mease RC, Pomper MG. A modular strategy to prepare multivalent inhibitors of prostate-specific membrane antigen (PSMA). *Oncotarget*. 2011; 2:1244–53. [PubMed: 22207391]
109. Behnam Azad B, Banerjee SR, Pullambhatla M, Lacerda S, Foss CA, Wang Y, et al. Evaluation of a PSMA-targeted BNF nanoparticle construct. *Nanoscale*. 2015; 7:4432–42. [PubMed: 25675333]
110. Taylor RM, Sillerud LO. Paclitaxel-loaded iron platinum stealth immunomicelles are potent MRI imaging agents that prevent prostate cancer growth in a PSMA-dependent manner. *Int J Nanomedicine*. 2012; 7:4341–52. [PubMed: 22915856]
111. Min K, Jo H, Song K, Cho M, Chun YS, Jon S, et al. Dual-aptamer-based delivery vehicle of doxorubicin to both PSMA (+) and PSMA (–) prostate cancers. *Biomaterials*. 2011; 32:2124–32. [PubMed: 21147500]
112. Yu MK, Kim D, Lee IH, So JS, Jeong YY, Jon S. Image-guided prostate cancer therapy using aptamer-functionalized thermally cross-linked superparamagnetic iron oxide nanoparticles. *Small*. 2011; 7:2241–9. [PubMed: 21648076]
113. Abdolahi M, Shahbazi-Gahrouei D, Laurent S, Sermeus C, Firozian F, Allen BJ, et al. Synthesis and in vitro evaluation of MR molecular imaging probes using J591 mAb-conjugated SPIONs for specific detection of prostate cancer. *Contrast Media Mol Imaging*. 2013; 8:175–84. [PubMed: 23281290]

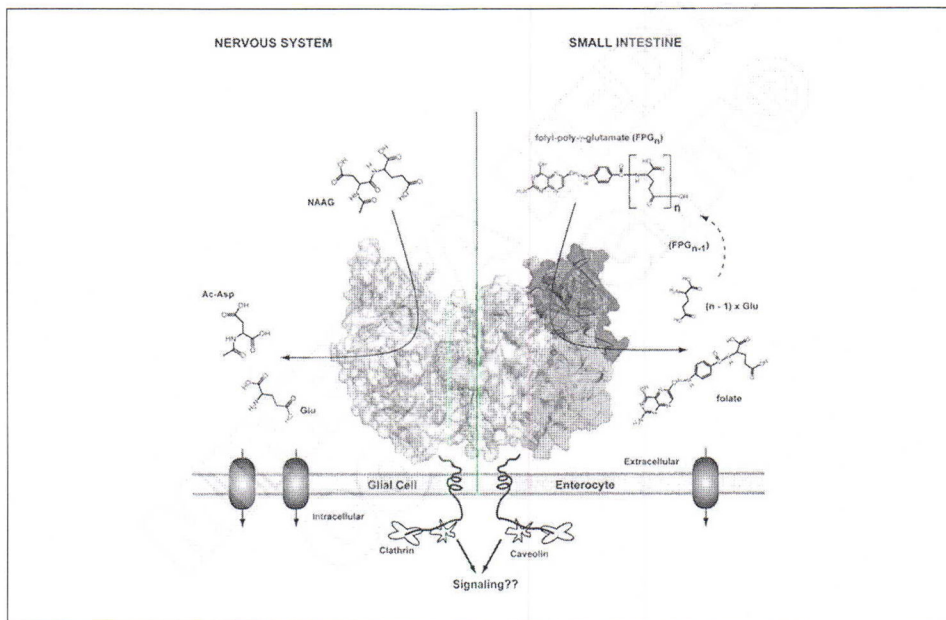


114. Tse BW, Cowin GJ, Soekmadji C, Jovanovic L, Vasireddy RS, Ling MT, et al. PSMA-targeting iron oxide magnetic nanoparticles enhance MRI of preclinical prostate cancer. *Nanomedicine (Lond)*. 2015; 10:375–86. [PubMed: 25407827]
115. Zhu Y, Sun Y, Chen Y, Liu W, Jiang J, Guan W, et al. In Vivo Molecular MRI Imaging of Prostate Cancer by Targeting PSMA with Polypeptide-Labeled Superparamagnetic Iron Oxide Nanoparticles. *Int J Mol Sci*. 2015; 16:9573–87. [PubMed: 25927579]
116. Banerjee SR, Ngen EJ, Rotz MW, Kakkad S, Lisok A, Pracitto R, et al. Synthesis and Evaluation of Gd(III)-Based Magnetic Resonance Contrast Agents for Molecular Imaging of Prostate-Specific Membrane Antigen. *Angew Chem Int Ed Engl*. 2015 Epub ahead of print.
117. Mastarone DJ, Harrison VS, Eckermann AL, Parigi G, Luchinat C, Meade TJ. A modular system for the synthesis of multiplexed magnetic resonance probes. *J Am Chem Soc*. 2011; 133:5329–37. [PubMed: 21413801]
118. Murphy GP, Maguire RT, Rogers B, Partin AW, Nelp WB, Troychak MJ, et al. Comparison of serum PSMA, PSA levels with results of Cytogen-356 ProstaScint scanning in prostatic cancer patients. *Prostate*. 1997; 33:281–5. [PubMed: 9397201]
119. Petronis JD, Regan F, Lin K. Indium-111 capromab pendetide (ProstaScint) imaging to detect recurrent and metastatic prostate cancer. *Clin Nucl Med*. 1998; 23:672–7. [PubMed: 9790041]
120. Sodee DB, Conant R, Chalfant M, Miron S, Klein E, Bahnson R, et al. Preliminary imaging results using In-111 labeled CYT-356 (Prostascint) in the detection of recurrent prostate cancer. *Clin Nucl Med*. 1996; 21:759–67. [PubMed: 8896922]
121. Bander NH, Trabulsi EJ, Kostakoglu L, Yao D, Vallabhajosula S, Smith-Jones P, et al. Targeting metastatic prostate cancer with radiolabeled monoclonal antibody J591 to the extracellular domain of prostate specific membrane antigen. *J Urol*. 2003; 170:1717–21. [PubMed: 14532761]
122. Osborne JR, Green DA, Spratt DE, Lyashchenko S, Fareedy SB, Robinson BD, et al. A prospective pilot study of (89)Zr-J591/prostate specific membrane antigen positron emission tomography in men with localized prostate cancer undergoing radical prostatectomy. *J Urol*. 2014; 191:1439–45. [PubMed: 24135437]
123. Pandit-Taskar N, O'Donoghue JA, Beylergil V, Lyashchenko S, Ruan S, Solomon SB, et al. (8) (9)Zr-huJ591 immuno-PET imaging in patients with advanced metastatic prostate cancer. *Eur J Nucl Med Mol Imaging*. 2014; 41:2093–105. [PubMed: 25143071]
124. Vallabhajosula S, Nikolopoulou A, Babich JW, Osborne JR, Tagawa ST, Lipai I, et al. 99mTc-labeled small-molecule inhibitors of prostate-specific membrane antigen: pharmacokinetics and biodistribution studies in healthy subjects and patients with metastatic prostate cancer. *J Nucl Med*. 2014; 55:1791–8. [PubMed: 25342385]
125. Cho SY, Gage KL, Mease RC, Senthamizhchelvan S, Holt DP, Jeffrey-Kwanisai A, et al. Biodistribution, tumor detection, and radiation dosimetry of 18F-DCFBC, a low-molecular-weight inhibitor of prostate-specific membrane antigen, in patients with metastatic prostate cancer. *J Nucl Med*. 2012; 53:1883–91. [PubMed: 23203246]
126. Rowe SPG, Macura K, Guner G, Faraj SF, Munari E, Rodriguez R, Han M, Blackford A, Netto G, Lodge M, Mease RC, Pomper MG, Cho SY. PSMA-based low molecular weight 18F-DCFBC PET/CT for detection and characterization of primary prostate cancer. *J Nucl Med*. 2015 Epub ahead of print.
127. Szabo Z, Mena E, Rowe SP, Plyku D, Nidal R, Eisenberger MA, et al. Initial evaluation of [18F] DCFPyL for prostate-specific membrane antigen (PSMA)-targeted PET imaging of prostate cancer. *Mol Imaging Biology*. 2015:1–10. Journal Article.
128. Beheshti M, Kunit T, Haim S, Zakavi R, Schiller C, Stephens A, et al. BAY 1075553 PET-CT for Staging and Restaging Prostate Cancer Patients: Comparison with [18F] Fluorocholine PET-CT (Phase I Study). *Mol Imaging Biology*. 2015; 17:424–33.
129. Eder M, Eisenhut M, Babich J, Haberkorn U. PSMA as a target for radiolabelled small molecules. *Eur J Nucl Med Mol Imaging*. 2013; 40:819–23. [PubMed: 23463331]
130. Sanchez-Crespo A. Comparison of Gallium-68 and Fluorine-18 imaging characteristics in positron emission tomography. *Applied radiation and isotopes: including data, instrumentation and methods for use in agriculture, industry and medicine*. 2013 Jun.76:55–62.

131. Afshar-Oromieh A, Zechmann CM, Malcher A, Eder M, Eisenhut M, Linhart HG, et al. Comparison of PET imaging with a (68) Ga-labelled PSMA ligand and (18)F-choline-based PET/CT for the diagnosis of recurrent prostate cancer. *Eur J Nucl Med Mol Imaging*. 2014; 41:11–20. [PubMed: 24072344]
132. Afshar-Oromieh A, Avtzi E, Giesel FL, Holland-Letz T, Linhart HG, Eder M, et al. The diagnostic value of PET/CT imaging with the (68)Ga-labelled PSMA ligand HBED-CC in the diagnosis of recurrent prostate cancer. *Eur J Nucl Med Mol Imaging*. 2015; 42:197–209. [PubMed: 25411132]
133. Eiber M, Maurer T, Souvatzoglou M, Beer AJ, Ruffani A, Haller B, et al. Evaluation of Hybrid 68Ga-PSMA Ligand PET/CT in 248 Patients with Biochemical Recurrence After Radical Prostatectomy. *J Nucl Med*. 2015; 56:668–74. [PubMed: 25791990]
134. Chakraborty PS, Kumar R, Tripathi M, Das CJ, Bal C. Detection of brain metastasis with 68Ga-labeled PSMA ligand PET/CT: a novel radiotracer for imaging of prostate carcinoma. *Clin Nucl Med*. 2015; 40:328–9. [PubMed: 25674861]
135. Afshar-Oromieh A, Haberkorn U, Hadaschik B, Habl G, Eder M, Eisenhut M, et al. PET/MRI with a 68Ga-PSMA ligand for the detection of prostate cancer. *Eur J Nucl Med Mol Imaging*. 2013; 40:1629–30. [PubMed: 23817686]
136. Eiber M, Nekolla SG, Maurer T, Weirich G, Wester HJ, Schwaiger M. Ga-PSMA PET/MR with multimodality image analysis for primary prostate cancer. *Abdom Imaging*. 2014 Epub ahead of print.
137. Uprimny C, Kroiss A, Nilica B, Buxbaum S, Decristoforo C, Horninger W, et al. (68)Ga-PSMA ligand PET versus (18)F-NaF PET: evaluation of response to (223)Ra therapy in a prostate cancer patient. *Eur J Nucl Med Mol Imaging*. 2015; 42:362–3. [PubMed: 25293866]
138. Dietlein M, Kobe C, Kuhnert G, Stockter S, Fischer T, Schomacker K, et al. Comparison of [F]DCFPyL and [Ga]Ga-PSMA-HBED-CC for PSMA-PET Imaging in Patients with Relapsed Prostate Cancer. *Mol Imaging Biol*. 26013479.
139. Deb N, Goris M, Trisler K, Fowler S, Saal J, Ning S, et al. Treatment of hormone-refractory prostate cancer with 90Y-CYT-356 monoclonal antibody. *Clin Cancer Res*. 1996; 2:1289–97. [PubMed: 9816299]
140. Kahn D, Austin JC, Maguire RT, Miller SJ, Gerstbrein J, Williams RD. A phase II study of [90Y] yttrium-capromab pendetide in the treatment of men with prostate cancer recurrence following radical prostatectomy. *Cancer Biother Radiopharm*. 1999; 14:99–111. [PubMed: 10850293]
141. Milowsky MI, Nanus DM, Kostakoglu L, Vallabhajosula S, Goldsmith SJ, Bander NH. Phase I trial of yttrium-90-labeled anti-prostate-specific membrane antigen monoclonal antibody J591 for androgen-independent prostate cancer. *J Clin Oncol*. 2004; 22:2522–31. [PubMed: 15173215]
142. Tagawa ST, Beltran H, Vallabhajosula S, Goldsmith SJ, Osborne J, Matulich D, et al. Anti-prostate-specific membrane antigen-based radioimmunotherapy for prostate cancer. *Cancer*. 2010; 116(4 Suppl):1075–83. [PubMed: 20127956]
143. Tagawa, ST.; Vallabhajosula, S.; Osborne, J.; Goldsmith, SJ.; Petrillo, K.; Tyrell, L., et al., editors. Phase I trial of fractionated-dose 177lutetium radiolabeled anti-prostate-specific membrane antigen (PSMA) monoclonal antibody J591 (177Lu-J591) in patients (pts) with metastatic castration-resistant prostate cancer (metCRPC); ASCO Annual Meeting Proceedings; 2010;
144. Watanabe R, Hanaoka H, Sato K, Nagaya T, Harada T, Mitsunaga M, et al. Photoimmunotherapy targeting prostate-specific membrane antigen: are antibody fragments as effective as antibodies? *J Nucl Med*. 2015; 56:140–4. [PubMed: 25500827]
145. Morris MJ, Divgi CR, Pandit-Taskar N, Batraki M, Warren N, Nacca A, et al. Pilot trial of unlabeled and indium-111-labeled anti-prostate-specific membrane antigen antibody J591 for castrate metastatic prostate cancer. *Clin Cancer Res*. 2005; 11:7454–61. [PubMed: 16243819]
146. Jeske, SJ.; Milowsky, MI.; Smith, CR.; Smith, KA.; Bander, NH.; Nanus, DM., editors. Phase II trial of the anti-prostate specific membrane antigen (PSMA) monoclonal antibody (mAb) J591 plus low-dose interleukin-2 (IL-2) in patients (pts) with recurrent prostate cancer (PC); ASCO Annual Meeting Proceedings; 2007;

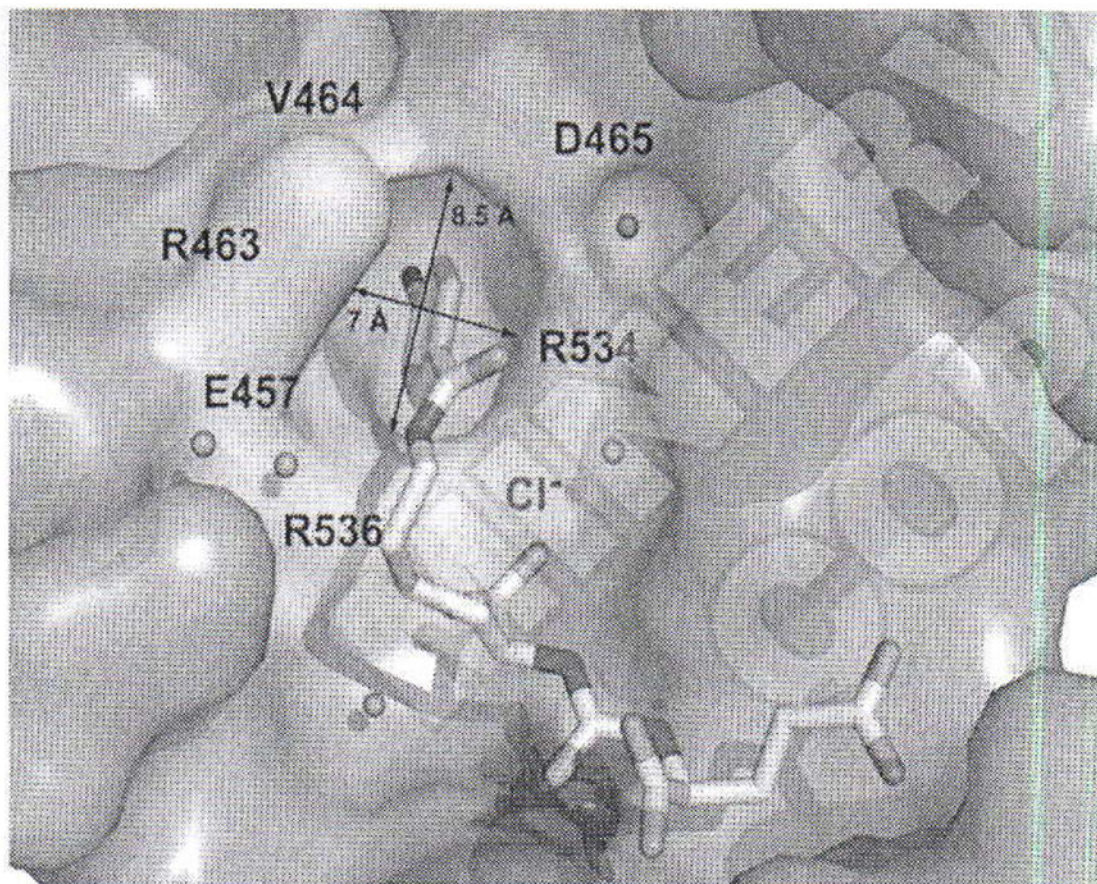
147. Hrkach J, Von Hoff D, Mukkaram Ali M, Andrianova E, Auer J, Campbell T, et al. Preclinical development and clinical translation of a PSMA-targeted docetaxel nanoparticle with a differentiated pharmacological profile. *Sci Transl Med*. 2012; 4:128ra39.
148. Galsky MD, Eisenberger M, Moore-Cooper S, Kelly WK, Slovin SF, DeLaCruz A, et al. Phase I trial of the prostate-specific membrane antigen-directed immunoconjugate MLN2704 in patients with progressive metastatic castration-resistant prostate cancer. *J Clin Oncol*. 2008; 26:2147–54. [PubMed: 18362364]
149. Henry MD, Wen S, Silva MD, Chandra S, Milton M, Worland PJ. A prostate-specific membrane antigen-targeted monoclonal antibody-chemotherapeutic conjugate designed for the treatment of prostate cancer. *Cancer Res*. 2004; 64:7995–8001. [PubMed: 15520207]
150. Milowsky, MI.; Galsky, M.; George, DJ.; Lewin, JM.; Rozario, CP.; Marshall, T., et al., editors. Phase I/II trial of the prostate-specific membrane antigen (PSMA)-targeted immunoconjugate MLN2704 in patients (pts) with progressive metastatic castration resistant prostate cancer (CRPC); ASCO Annual Meeting Proceedings; 2006;
151. Denmeade SR. Prostate-specific membrane antigen activated prodrug and imaging agents. Proceedings of the Innovative Minds in Prostate Cancer Today. 2011 IMPACT'11. Journal Article.
152. Petrylak, DP.; Kantoff, PW.; Frank, RC.; Shore, ND.; Rotshteyn, Y.; Israel, RJ., et al., editors. Prostate-specific membrane antigen antibody-drug conjugate (PSMA ADC): A phase I trial in taxane-refractory prostate cancer; ASCO Annual Meeting Proceedings; 2011;
153. Weineisen M, Schottelius M, Simecek J, Baum RP, Yildiz A, Beykan S, et al. 68Ga- and 177Lu-labeled PSMA I&T: Optimization of a PSMA targeted theranostic concept and first proof of concept human studies. *J Nucl Med*. 2015 Epub ahead of print.
154. Weineisen M, Simecek J, Schottelius M, Schwaiger M, Wester H-J. Synthesis and preclinical evaluation of DOTAGA-conjugated PSMA ligands for functional imaging and endoradiotherapy of prostate cancer. *EJNMMI Res*. 2014; 4:1–15. [PubMed: 24382020]
155. Baur B, Solbach C, Andreolli E, Winter G, Machulla HJ, Reske SN. Synthesis, Radiolabelling and In Vitro Characterization of the Gallium-68-, Yttrium-90- and Lutetium-177-Labelled PSMA Ligand, CHX-A''-DTPA-DUPA-Pep. *Pharmaceuticals (Basel)*. 2014; 7:517–29. [PubMed: 24787458]
156. Reske SN, Winter G, Baur B, Machulla HJ, Kull T. Comment on Afshar-Oromieh et al. PET imaging with a [68Ga]gallium-labelled PSMA ligand for the diagnosis of prostate cancer: biodistribution in humans and first evaluation of tumour lesions. *Eur J Nucl Med Mol Imaging*. 2013; 40:969–70. [PubMed: 23558687]
157. Kiess AP, Minn I, Chen Y, Hobbs R, Sgouros G, Mease RC, et al. Auger radiopharmaceutical therapy targeting prostate-specific membrane antigen. *J Nucl Med*. 2015 Epub ahead of print.
158. Banerjee SR, Foss CA, Pullambhatla M, Wang Y, Srinivasan S, Hobbs RF, et al. Preclinical evaluation of 86Y-labeled inhibitors of prostate-specific membrane antigen for dosimetry estimates. *J Nucl Med*. 2015; 56:628–34. [PubMed: 25722448]
159. Chen Z, Penet MF, Nimmagadda S, Li C, Banerjee SR, Winnard PT Jr, et al. PSMA-targeted theranostic nanoplex for prostate cancer therapy. *ACS Nano*. 2012; 6:7752–62. [PubMed: 22866897]
160. Wright GL Jr, Haley C, Beckett ML, Schellhammer PF. Expression of prostate-specific membrane antigen in normal, benign, and malignant prostate tissues. *Urol Oncol*. 1995; 1:18–28. [PubMed: 21224086]
161. Baccala A, Sercia L, Li J, Heston W, Zhou M. Expression of prostate-specific membrane antigen in tumor-associated neovasculature of renal neoplasms. *Urology*. 2007; 70:385–90. [PubMed: 17826525]
162. Wernicke AG, Edgar MA, Lavi E, Liu H, Salerno P, Bander NH, et al. Prostate-specific membrane antigen as a potential novel vascular target for treatment of glioblastoma multiforme. *Arch Pathol Lab Med*. 2011; 135:1486–9. [PubMed: 22032578]
163. Nomura N, Pastorino S, Jiang P, Lambert G, Crawford JR, Gymnopoulos M, et al. Prostate specific membrane antigen (PSMA) expression in primary gliomas and breast cancer brain metastases. *Cancer Cell Int*. 2014; 14:26. [PubMed: 24645697]

164. Haffner MC, Laimer J, Chau A, Schafer G, Obrist P, Brunner A, et al. High expression of prostate-specific membrane antigen in the tumor-associated neo-vasculature is associated with worse prognosis in squamous cell carcinoma of the oral cavity. *Mod Pathol.* 2012; 25:1079–85. [PubMed: 22460809]
165. Zeng C, Ke ZF, Yang Z, Wang Z, Yang SC, Luo CQ, et al. Prostate-specific membrane antigen: a new potential prognostic marker of osteosarcoma. *Med Oncol.* 2012; 29:2234–9. [PubMed: 22009216]
166. Wernicke AG, Varma S, Greenwood EA, Christos PJ, Chao KS, Liu H, et al. Prostate-specific membrane antigen expression in tumor-associated vasculature of breast cancers. *APMIS.* 2014; 122:482–9. [PubMed: 24304465]
167. Haffner MC, Kronberger IE, Ross JS, Sheehan CE, Zitt M, Muhlmann G, et al. Prostate-specific membrane antigen expression in the neovasculature of gastric and colorectal cancers. *Hum Pathol.* 2009; 40:1754–61. [PubMed: 19716160]
168. Wang, H-l; Wang, S-s; Song, W-h; Pan, Y.; Yu, H-p; Si, T-g, et al. Expression of Prostate-Specific Membrane Antigen in Lung Cancer Cells and Tumor Neovasculature Endothelial Cells and Its Clinical Significance. *PLoS ONE.* 2015:10.
169. Pandit-Taskar N, O'Donoghue JA, Divgi CR, Wills EA, Schwartz L, Gonen M, et al. Indium 111-labeled J591 anti-PSMA antibody for vascular targeted imaging in progressive solid tumors. *EJNMMI Res.* 2015; 5:28. [PubMed: 25984435]
170. Demirci E, Ocak M, Kabasakal L, Decristoforo C, Talat Z, Halac M, et al. (68)Ga-PSMA PET/CT imaging of metastatic clear cell renal cell carcinoma. *Eur J Nucl Med Mol Imaging.* 2014; 41:1461–2. [PubMed: 24756358]
171. Harada N, Kimura H, Ono M, Saji H. Preparation of asymmetric urea derivatives that target prostate-specific membrane antigen for SPECT imaging. *J Med Chem.* 2013; 56:7890–901. [PubMed: 24063417]
172. El-Zaria ME, Genady AR, Janzen N, Petlura CI, Beckford Vera DR, Valliant JF. Preparation and evaluation of carbonane-derived of prostate specific membrane antigen (PSMA). *Dalton Trans.* 2014; 43:4950–61. [PubMed: 24481236]



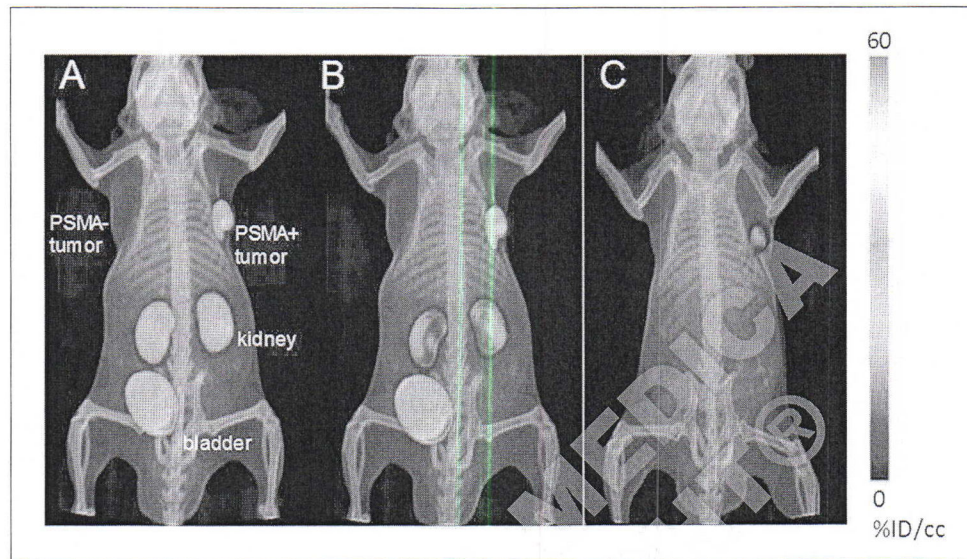
**Figure 1.** Homodimer of human PSMA (crystal structure) tethered to the biological membrane. One monomer shown in semitransparent surface representation with individual domains of the extracellular part colored green (protease domain; amino acids 57 – 116 and 352 – 590), blue (apical domain; amino acids 117 – 351), and yellow (C-terminal; amino acids 591 – 750); the second monomer is colored gray. *N*-linked sugar moieties are colored cyan, and the active-site Zn<sup>2+</sup> ions are shown as red spheres. Left panel: residing at the plasma membrane of astrocytes /schwann cells, PSMA catabolizes N-acetylaspartyl glutamate (NAAG), the most prevalent peptidic neurotransmitter in the mammalian nervous system. *N*-acetylaspartate and glutamate, the reaction products, are selectively transported into glial cells, metabolized and reused for NAAG synthesis in neurons. Right panel: PSMA (or folate hydrolase) at the plasma membrane of enterocytes in the proximal jejunum sequentially hydrolyzes the C-terminal  $\gamma$ -glutamate tail of dietary folates, finally leaving folate-monoglutamate, which can then be transported transcellularly into the blood stream [Adapted from Barinka C *et al.*].<sup>9</sup>



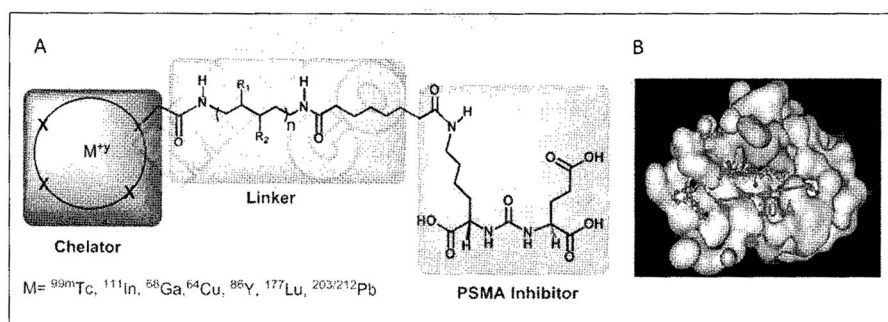


**Figure 2.** The hydrophobic pocket accessory to the S1 site. The active site bound DCIBzL is in stick representation. The dissected substrate-binding cavity of PSMA is shown in semi-transparent surface representation (gray). The side chains of amino acids delineating the “accessory hydrophobic pocket” are shown in stick representation and colored cyan. The active-site  $Zn^{+2}$  and S1 bound  $Cl^{-}$  are colored blue and represented as a transparent sphere, respectively and water molecules are shown as red spheres. Adapted from Barinka C *et al.*<sup>45</sup>

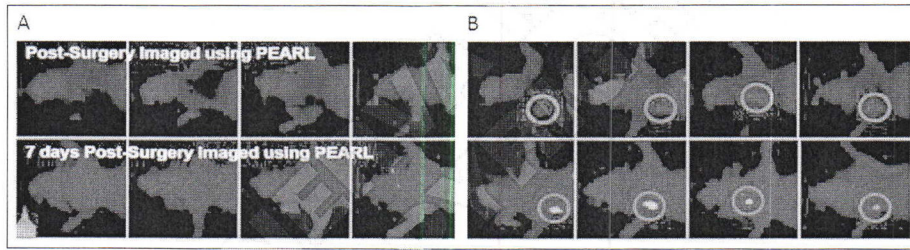




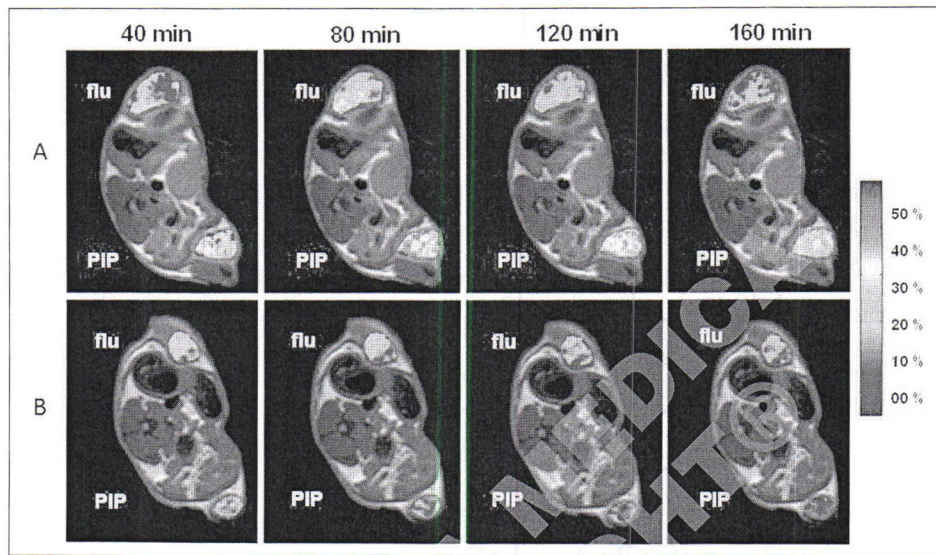
**Figure 3.** PET/CT volume-rendered composite images of [ $^{18}\text{F}$ ]DCFPyL in a mouse bearing PSMA+ PC3 PIP and PSMA- PC3 flu tumors at (A) 0–30 minutes; (B) 30–60 minutes and (C) 3–3.5 hours post-injection. By 30 minutes radiochemical uptake was evident within the PSMA+ PC3 PIP tumor and kidneys. Radioactivity receded from kidneys faster than from tumor, and was not evident within kidneys by 3.5 hours post-injection. Radioactivity within bladder was due to excretion. At no time was radioactivity clearly visualized within the isogenic, PSMA- PC3 flu tumor. Adapted from Chen Y *et al.*<sup>54</sup>



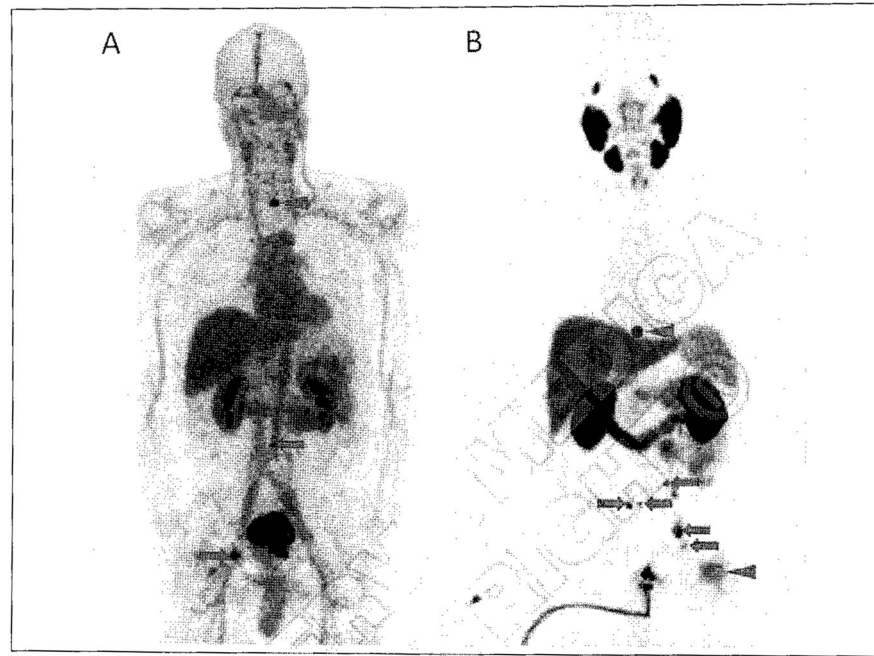
**Figure 4.** Long linker strategy for attachment of radiometals and other bulky substituents to PSMA-targeted, small-molecule agents. Tri-partite construct including the chelator, linker and targeting moiety (A). A minimal linker length of approximately 20Å enables productive binding of the construct to PSMA through externalization of the bulky substituent (B).



**Figure 5.** Near-infrared fluorescence) (NIRF) imaging with YC-27 Left panels show animals that underwent surgery with assistance of the Pearl imaging system to assure negative margins after receiving the PSMA-targeted NIRF agent, YC-27, while those on the right did not. Note re-growth of tumor as soon as seven days Post-operatively in the absence of NIR guidance (red circle, right panels) [Adapted from Neuman BP *et al*].<sup>104</sup>

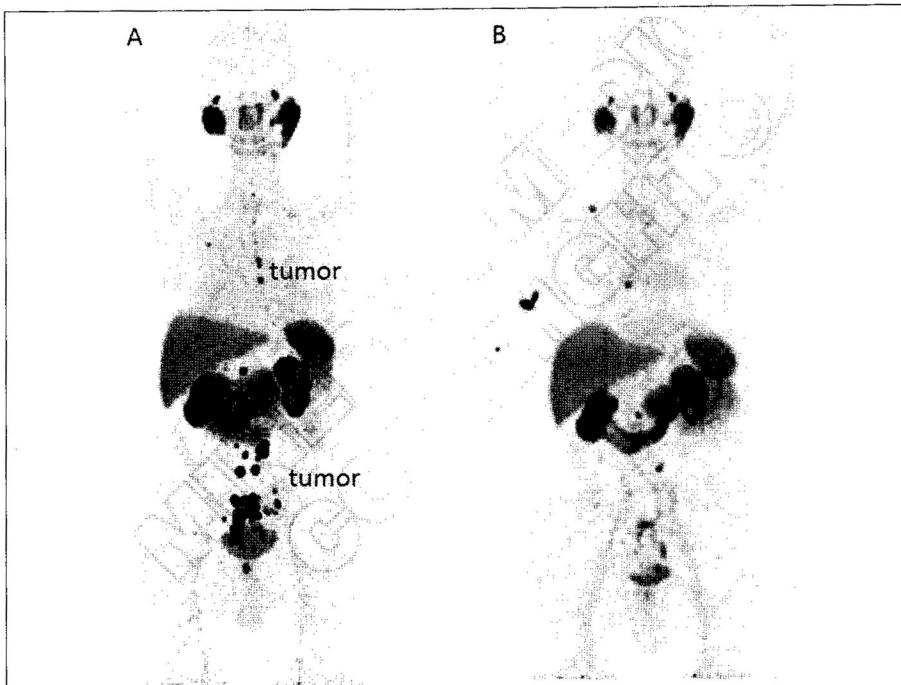


**Figure 6.** Compound Gd3 MR Imaging of human PSMA+ PC3 PIP and PSMA- PC3 flu tumor xenografts in male NOD/SCID mice. Enhancement ( $R_1\%$ ) maps in PSMA+ PC3 PIP and PSMA- PC3 flu tumors are superimposed upon  $T_2$ -weighted images during 40–160 min after a single bolus injection of Gd3 (A).  $R_1\%$  maps in PSMA+ PC3 PIP and PSMA- PC3 flu tumors of a trimeric Gd contrast agent without a PSMA-targeting moiety (B). [Adapted from Banerjee SR *et al.*]<sup>104</sup>



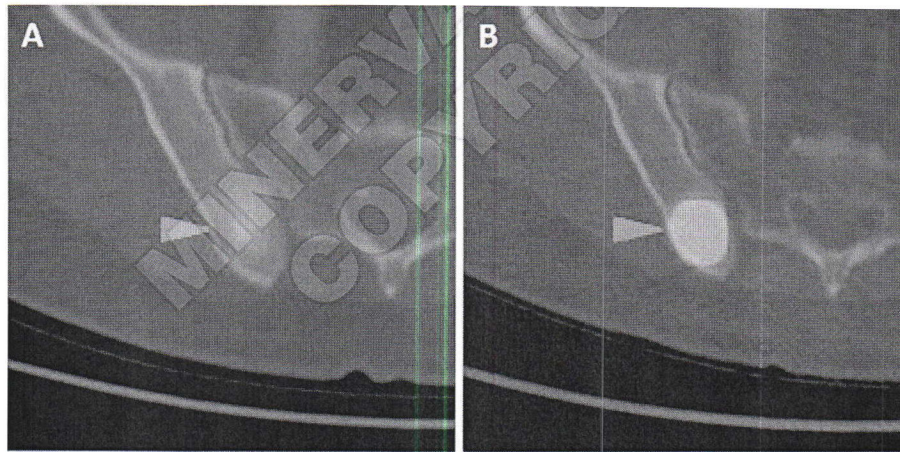
**Figure 7.** Maximum intensity projection images of patients with metastatic prostate cancer imaged with  $[^{18}\text{F}]\text{DCFBC}$  (A) and  $[^{18}\text{F}]\text{DCFPyL}$  (B). In both images, arrows demarcate sites of metastatic lymph nodes in the pelvis or retroperitoneum and arrowheads demonstrate sites of bone metastases (cervical spine in [A] and thoracic spine and left femoral head in [B]). Note the markedly reduced blood pool activity and overall higher tumor-to-background ratio with  $[^{18}\text{F}]\text{DCFPyL}$ .





**Figure 8.**  $^{68}\text{Ga}$ -PSMA PET/CT following therapy with  $^{177}\text{Lu}$ PSMA I&T. Patient presented with PSA=35.9 ng/mL and a PET scan showing multiple, intense mediastinal, abdominal and pelvic lymph node metastases, as well as lesions in the thoracic spine and local recurrence in the prostate fossa (A). Ten months later, after three cycles of peptide radioligand therapy (PRLT) PSA decreased to 1.0 ng/mL with significant regression of previously noted disease (B). Three foci of radioactivity superimposed upon the thorax are due to retention of radioactivity within the Port-A-Cath<sup>®</sup> device in B. Images courtesy Dr. Richard Baum, Zentralklinik Bad Berka, DE.

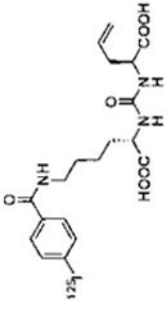
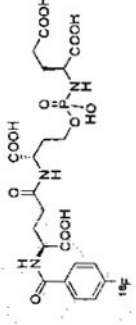
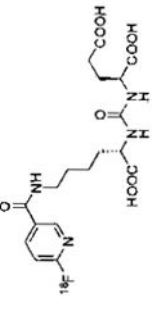
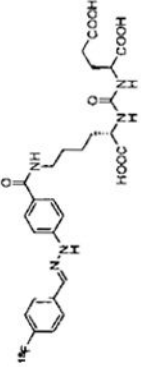
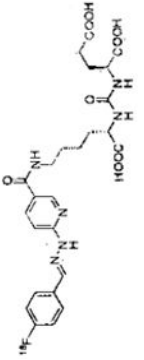
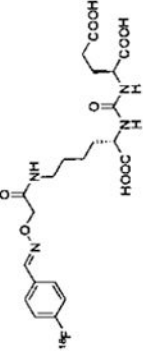
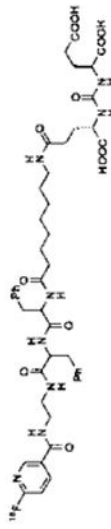
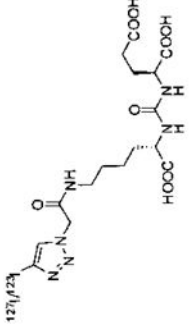
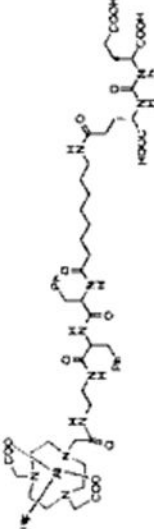
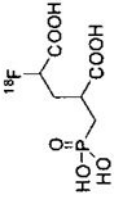


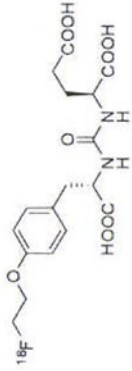
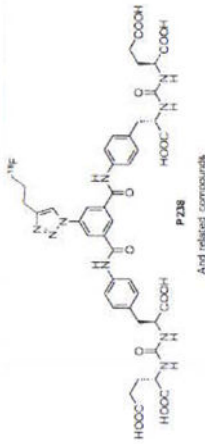
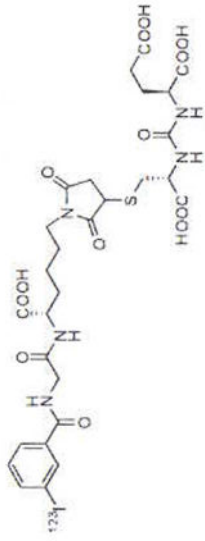
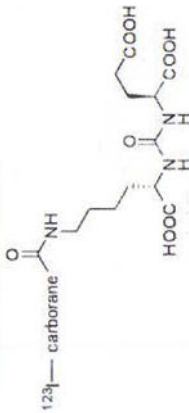
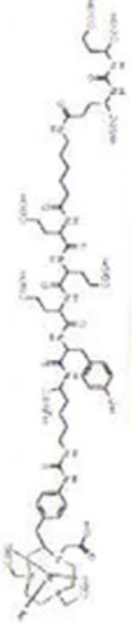
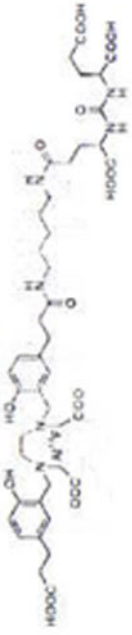
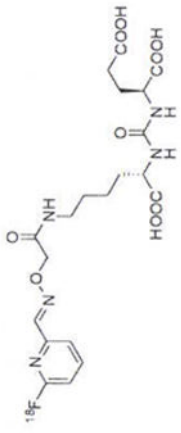
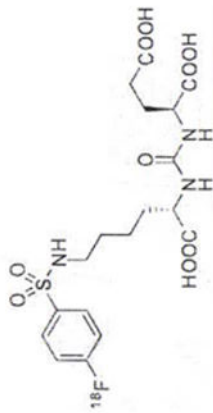


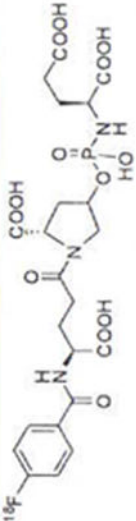
**Figure 9.** Axial FDG PET/CT (A) and axial [ $^{18}\text{F}$ ]DCFPyL PET/CT (B) images of a patient with metastatic clear cell renal cell carcinoma involving the posterior aspect of the right iliac bone. Both images are set to the same quantitative scale, highlighting the increased tumor uptake achieved with [ $^{18}\text{F}$ ]DCFPyL in this case.

**Table I**  
Carbon-11 and Radiohalogen-based, PSMA-targeted PET and SPECT imaging agents.

Entry	Structure	Ref.	Entry	Structure	Ref.
1		51	2		52
3		53	4		46
5		46	6		46
7		68	8		69

Entry	Structure	Ref.	Entry	Structure	Ref.
9		49	10		64
11		54	12		55
13		55	14		55
15		57	16		70
17		59	18		66

Entry	Structure	Ref.	Entry	Structure	Ref.
19		61	20		62
21		171	22		172
23		59	24		60
25		56	26		56

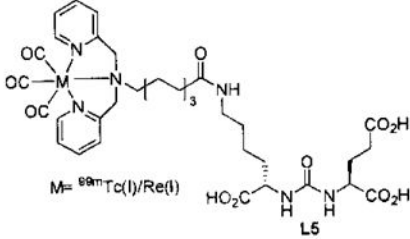
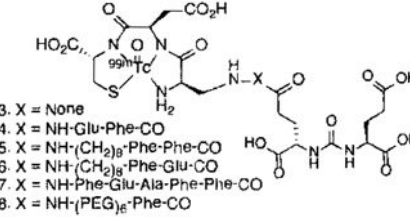
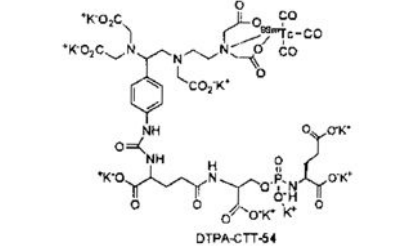
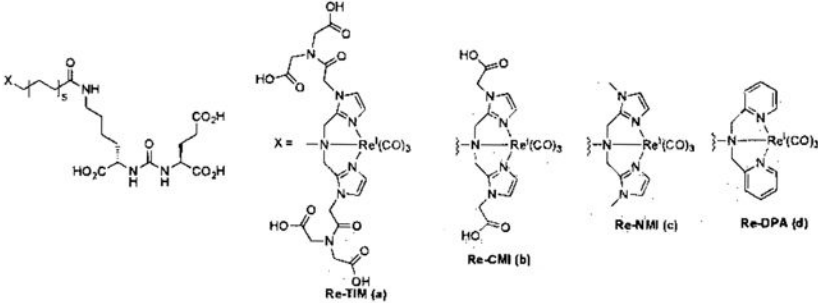
Entry	Structure	Ref. Entry	Structure	Ref.
27		65		

**Table II**

Radiometal-based, PSMA-targeted PET and SPECT imaging agents.

Entry	Structure	References
1	<p style="text-align: center;"><b>a</b></p> <p style="text-align: center;"><b>b</b>      <b>c</b>      <b>d</b></p>	81
2	<p style="text-align: center;"><math>M = {}^{99m}\text{Tc(I)} / \text{Re(I)}</math></p> <p style="text-align: center;"><b>L1-L3</b></p> <p style="text-align: center;">L1, <math>R_1 = R_2 = \text{Py}</math>, <math>R_3 = \text{H}</math>, <math>R_4 = \text{CO}_2\text{H}</math>  L2, <math>R_1 = R_2 = \text{Q}</math>, <math>R_3 = \text{H}</math>, <math>R_4 = \text{CO}_2\text{H}</math>  L3, <math>R_1 = R_2 = \text{Py}</math>, <math>R_3 = \text{CO}_2\text{H}</math>, <math>R_4 = \text{H}</math></p>	73
3	<p style="text-align: center;"><b>L4, L7</b></p> <p style="text-align: center;">L4, <math>R = \text{CO}_2\text{H}</math>  L7, <math>R = \text{Py}</math></p>	73



Entry	Structure	References
4	 <p><math>M = {}^{99m}\text{Tc(I)}/\text{Re(I)}</math></p> <p>L5</p>	73
5	 <p>3. X = None            4. X = NH-Glu-Phe-CO            5. X = NH-(CH<sub>2</sub>)<sub>6</sub>-Phe-Phe-CO            6. X = NH-(CH<sub>2</sub>)<sub>6</sub>-Phe-Glu-CO            7. X = NH-Phe-Glu-Ala-Phe-Phe-CO            8. X = NH-(PEG)<sub>6</sub>-Phe-CO</p>	75
6	 <p>DTPA-CTT-54</p>	79
7	 <p>Re-TIM (a)</p> <p>Re-CMI (b)</p> <p>Re-NMI (c)</p> <p>Re-DPA (d)</p>	76

Entry	Structure	References
8	<p><math>^{99m}\text{Tc}(\text{CO})_3\text{-DPA-DBCO-PEG}_4\text{-CTT-54}</math></p>	80
9	<p>Y-Linker-Tether</p> <p>Re-TIM (a), Re-CMI (b), Re-NMI (c), Re-DPA (d)</p>	77
10	<p>MIP-1404, MIP-1405</p>	78, 124
11	<p><math>[^{99m}\text{Tc}]L_8</math>, <math>[^{99m}\text{Tc}]L_9</math>, <math>[^{99m}\text{Tc}]L_{10}</math></p>	74

Entry	Structure	References
12	<p>MAG-2 <math>[^{99m}\text{Tc}]</math>L11, no X  <math>[^{99m}\text{Tc}]</math>L12, X = Phe  <math>[^{99m}\text{Tc}]</math>L13, X = Phe-Phe</p> <p>MAG-2 <math>[^{99m}\text{Tc}]</math>L14</p> <p>MAG-3 <math>[^{99m}\text{Tc}]</math>L15</p> <p>Diamidodithiol <math>[^{99m}\text{Tc}]</math>L16</p> <p>Diamide-monocysteine-thiol <math>[^{99m}\text{Tc}]</math>L17, X = H  <math>[^{99m}\text{Tc}]</math>L18, X = <math>\text{CH}_2\text{CO}_2\text{H}</math></p>	74
13	<p><math>\text{R}_1</math></p> <p><math>\text{R}_1 =</math> a, b, c</p>	92
14	<p><math>\text{Cu}^{2+}</math></p>	92

Author Manuscript

Author Manuscript

Author Manuscript

Author Manuscript

**Table III**

Radiometal-based, PSMA-targeted theranostics

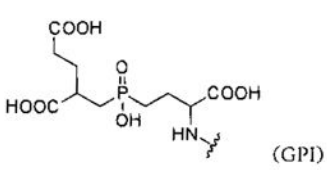
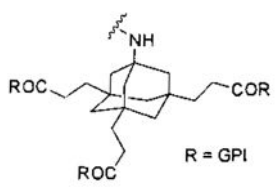
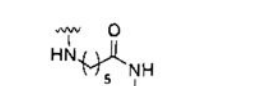

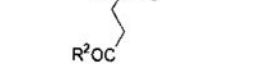
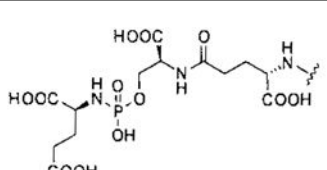
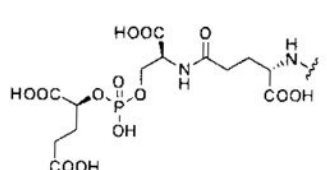
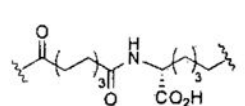
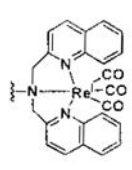
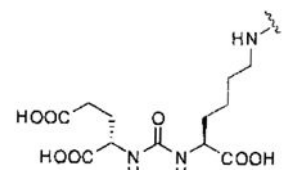
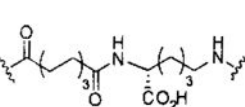
Compound	Entry	References
	1	82
<p><math>M = {}^{68}\text{Ga}/{}^{64}\text{Cu}/{}^{86}\text{Y}</math> 2-4      <math>M = {}^{68}\text{Ga}/{}^{177}\text{Lu}</math> 5</p>	2-4 5	82, 92, 175 153, 154
<p><math>M = {}^{111}\text{In}, {}^{86}\text{Y}, {}^{177}\text{Lu}</math></p>	6-8	158, 108
<p><math>{}^{68}\text{Ga}</math>-DKFZ-PSMA-11</p>	9	83





**Table IV**

Optical agents targeting PSMA

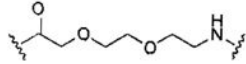
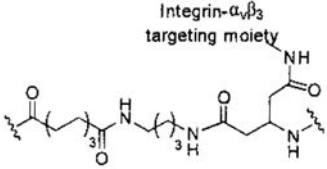
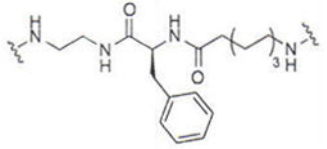
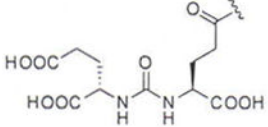
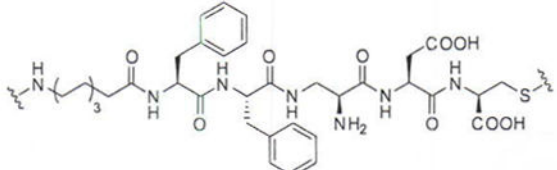
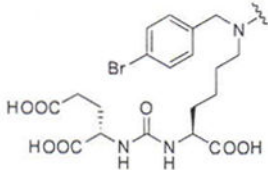
Inhibitor	Entry	Linker	Fluorophore	Reference
	1	No linker	IRDye78	98
	2	No linker	IRDye800CW	99
	3	 R = GPI	IRDye800RS	99
	4	 R <sup>1</sup> , R <sup>2</sup> = H; R <sup>3</sup> = GPI		
	5	 R <sup>1</sup> = H; R <sup>2</sup> , R <sup>3</sup> = GPI	IRDye800CW	99
	6	 R <sup>1</sup> , R <sup>2</sup> , R <sup>3</sup> = GPI		
	7	No linker	5-FAM-X	40
	8	No linker	5-FAM	100
	9	PEG <sub>3</sub>	5-FAM	100
	10	No linker	Cy5.5	101
	11			73
	12		IRDye800CW	102
	13		IRDye800RS	103
	14		ICG derivative	103
	15		Cy7	103
	16		Cy5.5	103
	17	No linker	IRDye800CW	103
	18	No linker	IRDye800RS	103

Author Manuscript

Author Manuscript

Author Manuscript

Author Manuscript

Inhibitor	Entry	Linker	Fluorophore	Reference
	19		ICG derivative	103
	20		Cy7	103
	21		Cy5.5	103
	22		IRDye800CW	103
	23		IRDye800RS	103
	24		ICG derivative	103
	25		Cy7	103
	26		Cy5.5	103
	27		IRDye800CW	107
	28		FITC	75
	29		Rhodamine B	75
	30		DyLight 680	105
	31		Alexa Fluor 647	105
	32		IRDye800CW	105
	33	Amc-Ahx-Glu-Glu-Glu-Lys	IRDye800CW	106
	34		5(6)-FAM	48

Author Manuscript

Author Manuscript

Author Manuscript

Author Manuscript